PhotoScience Advances
https://www.sciltp.com/journals/psa

Review

Recent Progress in the Development of Small Molecule-Based Fluorescent Probes for Oxidative Stress

Yusheng Fan, Yanlin Fu, Chunfei Bao and Yubin Ding *

Department of Chemistry, College of Sciences, Nanjing Agricultural University, Nanjing 210095, China
* Correspondence: ybding@njau.edu.cn

How To Cite: Fan, Y.; Fu, Y.; Bao, C.; et al. Recent Progress in the Development of Small Molecule-Based Fluorescent Probes for Oxidative Stress. *PhotoScience Advances* **2025**, *1*(1), 3.

Received: 30 August 2025
Revised: 26 September 2025
Accepted: 9 October 2025
Published: 17 October 2025

Abstract: Oxidative stress, driven by overproduction of reactive oxygen and nitrogen species, is implicated in numerous diseases. The precise detection of oxidative stress biomarkers is therefore crucial for understanding their biological roles. In this review, we intend to discuss recent advances in the development of fluorescent probes for detecting oxidative stress-related analytes. We specifically highlight the design strategies, sensing mechanisms, and performance of recently reported probes for hypochlorite and peroxynitrite, and other important ROS/RNS. The discussion is divided into four subtopics including fluorescent probes for hypochlorite, fluorescent probes for peroxynitrite, fluorescent probes for other oxidative stress species and fluorescent probes for multiple oxidative stress related analytes. Especially, we are interested in probes with multi-analyte responsive abilities, which are even capable of differentiating between multiple ROS/RNS. We propose that the comprehensive measurement of multiple biomarkers represents a critical future direction for this field. With a well-designed chemical structure, these probes are not just analytical tools. They are translational bridges that transform our understanding of oxidative stress into actionable clinical insights for earlier diagnosis, mechanistic understanding, and therapeutic monitoring.

Keywords: fluorescent probe; dye; oxidative stress; ROS; RNS

1. Introduction

Oxidative stress, resulted by over production of reactive oxygen and nitrogen species (ROS/RNS), is a crucial physiological and pathological process [1]. It is intrinsically linked to a myriad of diseases, including neurodegenerative disorders, cancer, inflammatory conditions, and cardiovascular ailments [2]. Key reactive species such as hypochlorous acid/hypochlorite ($HOCl/ClO^-$), peroxynitrite ($ONOO^-$), hydrogen peroxide (H_2O_2), and hydroxyl radical (•OH) are central mediators of oxidative damage (Table 1), thus their precise roles, concentrations, and spatiotemporal relationships within living systems are of great research interest [3]. To unravel this complexity, the development of reliable analytical tools for the real-time tracking of these molecules is of paramount importance [4].

Among various detection techniques, fluorescence imaging utilizing small organic molecule-based probes has emerged as a preeminent method due to its exceptional advantages [5–7]. Particularly, small-molecule probes are typically easy to synthesize, modify, and scale up, offering greater versatility and accessibility for a wide range of research applications [8,9]. Their small size minimizes steric interference and facilitates efficient cellular uptake, enabling real-time, non-invasive monitoring of biological processes within living systems [10]. In addition, their pronounced fluorescence changes provide a highly sensitive and easily detectable signal [11]. These advantages make small organic molecule-based probes indispensable tools for chemical biology and bioimaging [12].

This review aims to summarize and discuss the very recent advancements in the design, sensing mechanisms, and applications of small organic molecule-based fluorescent sensors for the detection of oxidative stress

biomarkers. The article is systematically organized into four sections to provide a comprehensive overview: (i) fluorescent probes for the detection of ClO^-; (ii) fluorescent probes for $ONOO^-$; (iii) fluorescent probes for other significant oxidative stress species, including H_2O_2 and •OH; and (iv) multi-analyte responsive probes capable of differentiating between two or more species, which represent the cutting edge in understanding the interconnected network of oxidative stress. Through this critical examination, we highlight the current state of the art and offer perspectives on future challenges and opportunities in this important research field.

Table 1. Common reactive oxygen and nitrogen species involved in oxidative stress.

Species	Biological Sources	Characteristics & Biological Roles
$O_2•^-$	Mitochondrial electron transport chain, NADPH oxidase enzymes	The primary ROS, formed by one-electron reduction of O_2. Acts as a signaling molecule but can damage iron-sulfur cluster proteins. A precursor to most other ROS.
H_2O_2	Dismutation of $O_2•^-$	A major redox signaling agent. At high levels, it contributes to oxidative damage.
•OH	Fenton reaction	Reacts instantaneously with all biomolecules, causing severe and indiscriminate damage.
ClO^-	Myeloperoxidase-catalyzed reaction of H_2O_2 with Cl^- ions	A potent antibacterial agent produced by neutrophils.
•NO	Nitric oxide synthases	A crucial gaseous signaling molecule regulating vasodilation, neurotransmission, and immune response.
$ONOO^-$	Reaction between •NO and $O_2•^-$	A highly potent and damaging oxidant.

2. Fluorescent Probes for ClO^-

Hypochlorous acid, produced by white blood cells, is a crucial biological signaling molecule. It works as a primary defense against pathogens and is essential for our immune system [13]. However, excessive or misregulated production of ClO^- can lead to oxidative stress, causing significant damage to tissues and biomolecules like proteins, lipids, and DNA due to its highly reactive nature [14]. This damage could be implicated in the progression of numerous inflammatory diseases, including atherosclerosis, rheumatoid arthritis, and neurodegenerative disorders. Consequently, the quantitative detection of ClO^- is vital for diagnosing the related diseases. For the development of fluorescent sensors for ClO^-, ClO^- induced deprotection reaction is an effective strategy to design the sensor molecule.

For the design of fluorescent probes for ClO^-, thiocarbamate group can be considered as an ideal selective recognition unit. An activable near-infrared (NIR) fluorescent probe **Cy-DM** was designed by Wang et al. for rapid recognition of ClO^- in vivo (Figure 1a) [15]. In the design, D-mannosamine was used as a targeting group, which enhances its localization on inflammatory cells. Additionally, they selected thiocarbamate phenyl fragment as the recognition group, which would be cleaved upon interaction with ClO^-. The probe **Cy-DM** is initially non-fluorescent. However, upon the introduction of ClO^-, significant fluorescence enhancement was observed due to the intramolecular charge transfer mechanism. **Cy-DM** can rapidly recognize ClO^- within two seconds, with a detection limit as low as 0.84 μM. Furthermore, it exhibits an increased Stokes shift during the recognition process. The authors also highlighted **Cy-DM's** promising potential for applications in mouse models of inflammatory bowel disease (IBD) and in vitro testing.

Li et al. designed a fluorescent probe named **OPD**, to detect ClO^- in senescent cells and living organisms (Figure 1b) [16]. The researchers selected dicyanoisofluorone with a D-π-A structure as the fluorophore and modified it with 2-amino-5-chlorobenzamide to achieve a longer emission wavelength. The dimethylamino thiocarbamoyl (DMTC) unit was incorporated as the recognition site. Upon the addition of ClO^-, the recognition group underwent hydrolysis, which restores the ICT effect and reactivates the fluorescence of the probe ($\lambda\ max_{em}$ = 682 nm). With its high sensitivity to ClO^-, the probe successfully identified elevated ClO^- levels in drug-induced senescent cells and demonstrated effective imaging in zebrafish and mouse models, revealing increased ClO^- content in senescent organisms.

Yu et al. developed a NIR fluorescent probe **DL-Cl** for noninvasive evaluation of cancer-therapy responses to ferroptosis through real-time HClO imaging (Figure 1c) [17]. This probe featured a hemicyanine skeleton with a chlorine atom and a methylparaben group, which were quenched by dimethylthiocarbamate. Upon exposure to ClO^-, the probe specifically emitted fluorescence emission at 740 nm. The probe exhibited high sensitivity and specificity, with a detection limit of 0.32 μM for ClO^- and a rapid response time of 2.5 min. **DL-Cl** enabled real-time monitoring of ClO^- dynamics in various ferroptosis-triggering pathways and demonstrated superior

performance in tumor identification, facilitating image-guided tumor resection and ferroptosis-mediated tumor therapy evaluation.

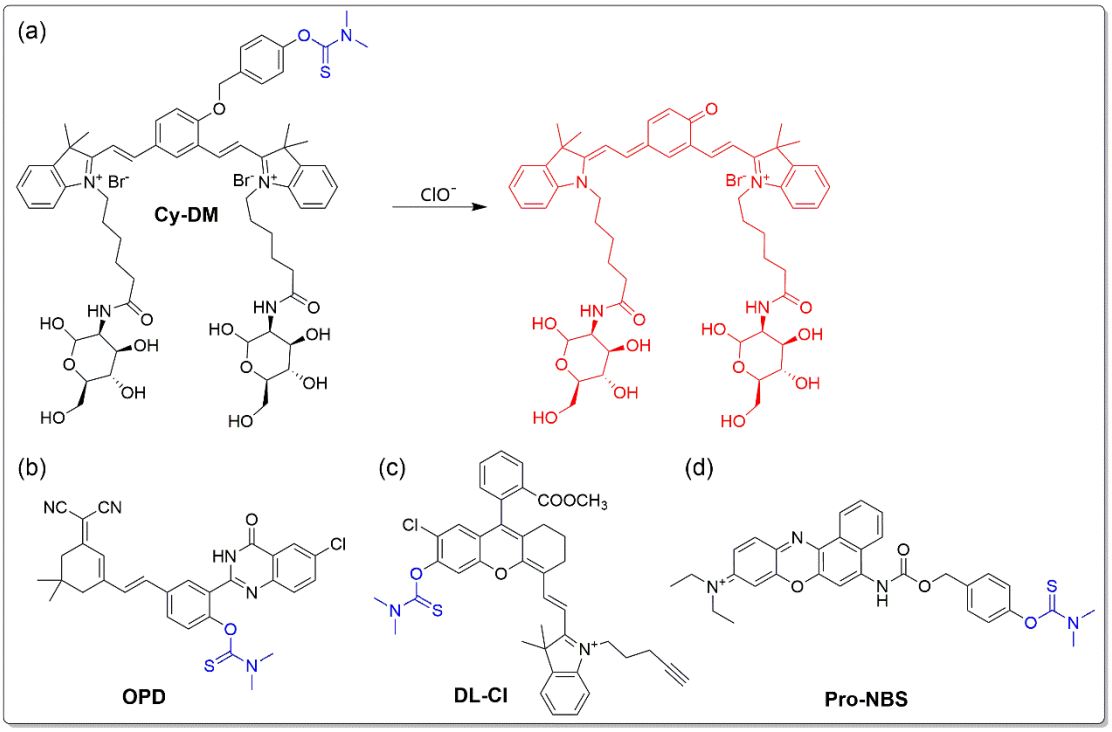

Figure 1. (**a**) Recognition mechanism of **Cy-DM** toward ClO^-; (**b**) Chemical structure of probe **OPD**; (**c**) Chemical structure of probe **DL-Cl**; (**d**) Chemical structure of probe **Pro-NBS**.

Zhang et al. developed a fluorescent probe, **Pro-NBS**, with specific selectivity for ClO^- by incorporating N,N-dimethylsulfanyl as the recognition group and Nile blue fluorophore as the reporter group (Figure 1d) [18]. Fluorescence titration analysis demonstrated a significant fluorescence enhancement upon the addition of ClO^- to the **Pro-NBS** probe, exhibiting a strong linear relationship, with a detection limit as low as 6 nM. Furthermore, the probe features a long emission wavelength and qualifies as a near-infrared fluorescent probe, making it suitable for detecting ClO^- both in vivo and in vitro. The authors further illustrated that the **Pro-NBS** probe can be effectively employed to monitor changes in ClO^- concentration in keloids and to assess the differences between normal fibroblasts and keloid-derived fibroblasts.

Yang et al. reported a two-photon ratiometric fluorescent probe **SRF-ClO** for the detection of ClO^- (Figure 2) [19]. The design strategy hinged on incorporating a tetrahydroquinoxaline group as an electron donor within a coumarin derivative, which strengthened the ICT effect to get a larger Stokes shift. When the probe reacted with ClO^-, the thioether bond was broken to generate the product as **SRF**. The probe's fluorescence emission color shifted from orange (λ_{em} = 583 nm) to red (λ_{em} = 650 nm), realizing a ratiometric detection. The detection limit of the probe for ClO^- is 2.7 nM, which is determined based on a signal-to-noise ratio of 3. Based on these characteristics, the probe has been successfully applied to super-resolution image of lysosomal ClO^- in cells undergoing ferroptosis.

Hua et al. synthesized a multifunctional fluorescent probe, **PNPM**, for the sensitive and selective detection of ClO^- by selecting N-annulated perylene (NP) as a fluorophore and coupling it with malononitrile as a recognition component for ClO^- (Figure 3) [20]. Due to the process of photo-induced electron transfer (PET), the probe became pH sensitive. The probe **PNPM** is inherently non-fluorescent in neutral environments, but upon addition of ClO^-, there is an intense yellow fluorescence emission at 535 nm. However, under weakly acidic conditions, the probe **PNPM** has an intense red fluorescence at approximately 650 nm. As the ClO^- concentration increases, the fluorescence gradually changes to yellow. The favorable change in ratiometric fluorescence is conducive to improved immunity to interference and reduced LOD (15.3 nM). This phenomenon suggests that the fluorescent probe **PNPM** has the ability to simultaneously monitor ClO^- concentration and pH.

Liu et al. developed a simple ratiometric NIR fluorescent probe **Nap-DCE**, which contains conjugated 1,8-naphthimide and dicyanoisophorone building blocks for the detection of ClO^- (Figure 4) [21]. The sensing mechanism involves the release of 1,8-naphthimide fluorophore in the presence of ClO^-, which process resulted in inhibition of the ICT process from the electron donor 1,8-naphthimide to the acceptor dicyanoisophorone. Fluorescent

probe **Nap-DCE** has high selectivity, sensitivity, good biocompatibility, and low detection limit (LOD = 0.738 μM) for ClO^- sensing. The naked eye ClO^- detection can be achieved via fluorescence ratio manner. The probe showed a fast response toward ClO^- that can be accomplished in less than 3 s. In addition, the application of **Nap-DCE** loaded paper sensing has a modest 'naked eye' color change to ClO^-.

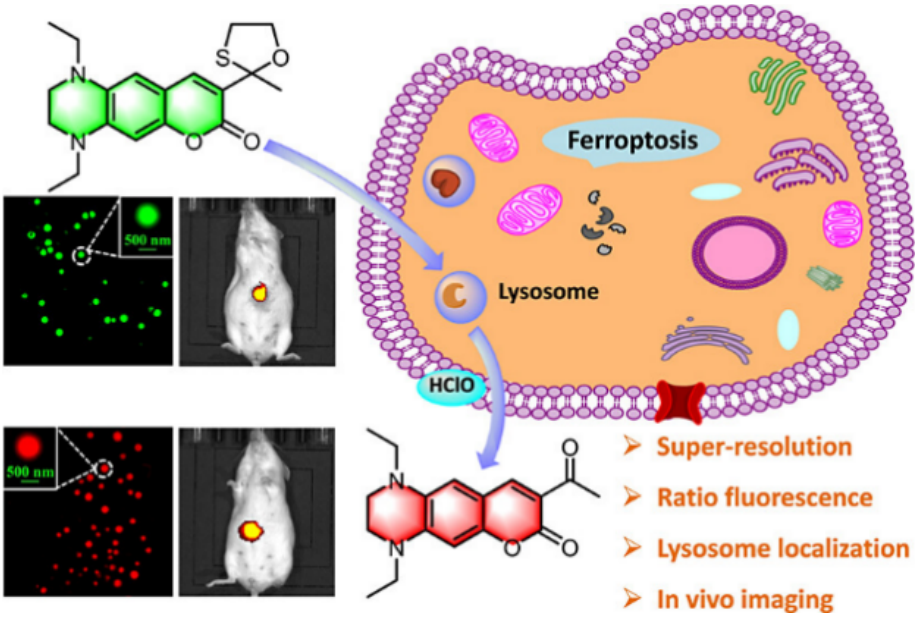

Figure 2. Proposed mechanism for **SRF-ClO**. Reproduced with permission [19]. Copyright 2024, American Chemical Society.

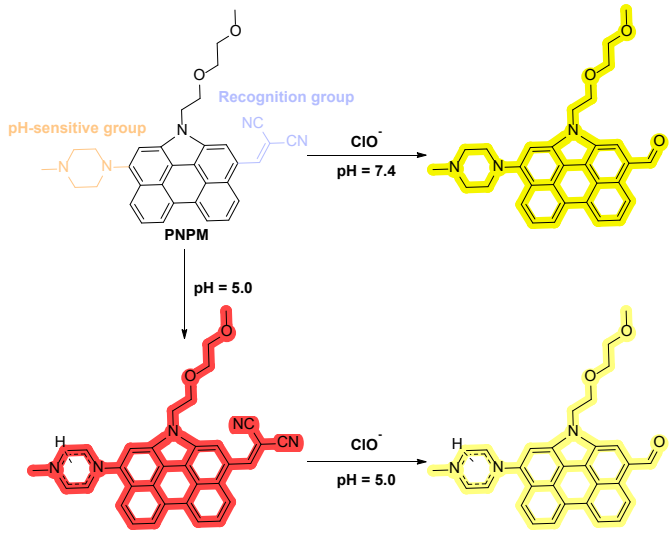

Figure 3. The chemical structure of probe **PNPM** and its ClO^- sensing mechanism.

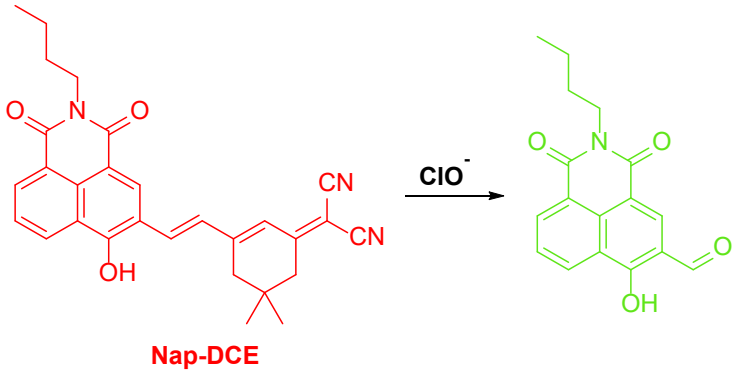

Figure 4. Sensing mechanism of **Nap-DCE** for the detection of ClO^-.

Mahapatra et al. prepared a near-infrared (NIR) fluorescent "turn-on" probe, **BPH**, for selectively recognizing ClO^- (Figure 5) [22]. The probe **BPH** is initially non-fluorescent due to the photo-induced electron transfer (PET) effect. Upon the addition of ClO^-, the o-diol in the induced structure undergoes oxidation to form a benzoquinone group, which suppresses the PET effect and results in the emission of a more pronounced red fluorescence. Optical property assessments demonstrated that **BPH** exhibits excellent selectivity for ClO^-. As the concentration of ClO^- increases, the intensity of the red fluorescence becomes increasingly pronounced, showing a strong linear relationship with ClO^- concentration, and achieving a detection limit as low as 0.23 nM. Furthermore, **BPH** not only demonstrates impressive performance in solution but also holds significant potential for applications in in vivo cellular testing.

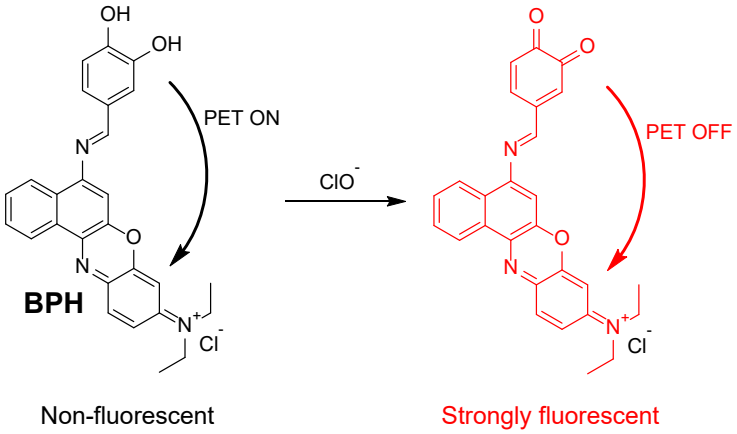

Figure 5. Recognition mechanism of **BPH**.

In addition to above mentioned deprotection strategy, the oxidation activity of ClO^- could also be used for the design of its fluorescent sensors. For example, Wang et al. presented a NIR ratiometric fluorescent probe **GA-BOD-S** for the detection of ClO^- in cancer cells (Figure 6) [23]. The probe, based on BODIPY and phenothiazine, targeted the Golgi apparatus and exhibited high sensitivity, a low detection limit of 35 nM, and rapid response time within 13 s. The combination of BODIPY and phenothiazine in the probe induced ICT effect, which extended the fluorescence emission wavelength into the near-infrared region. The sulfur atom in the phenothiazine can be oxidized into a sulfoxide by ClO^-, leading to a shift in fluorescence emission from 752 nm to 681 nm due to the disruption of the ICT effect. This change enabled ratiometric detection. Additionally, with the addition of ClO^-, the absorption peak shifted from 721 nm to 628 nm, and the solution colour changes from green to dark blue. These resulted demonstrate that the probe can recognize ClO^- through both ratiometric and colorimetric dual modes. It was worth mentioning that **GA-BOD-S** effectively differentiated the baseline ROS levels between tumor cells and normal cells through ratiometric fluorescence imaging.

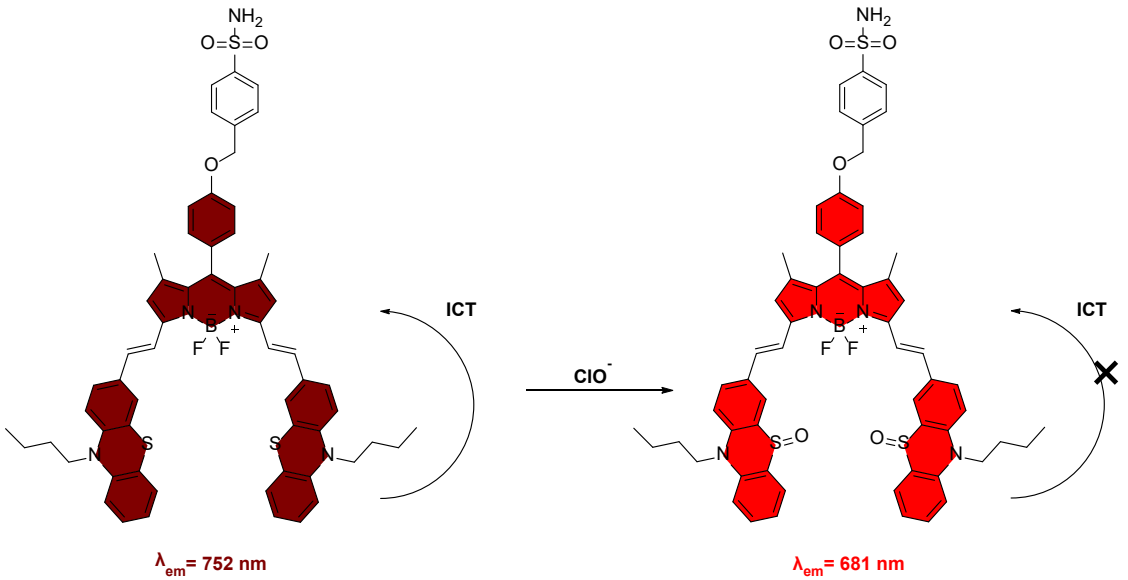

Figure 6. Proposed mechanism for **GA-BOD-S**.

Zhang et al. developed a ratiometric fluorescent probe, **YM-P**, for imaging of mitochondrial ClO^- during ferroptosis (Figure 7) [24]. This probe incorporates a triphenylphosphine group for specific mitochondrial targeting and a chloroacetyl chloride group for covalent binding, ensuring stable labeling even when the mitochondrial membrane potential fluctuates. The introduction of phenothiazine into the coumarin structure not only served as a recognition site for the probe but also endowed it with a larger stokes shift of 210 nm. The probe itself exhibited fluorescence at 650 nm. As the divalent sulfur atom was oxidized to sulfoxide by ClO^-, a new fluorescence emission emerged at 520 nm, thereby enabling ratiometric detection of ClO^- with a low detection limit of 35 nM. Utilizing **YM-P**, the researchers achieved dynamic super-resolution imaging of mitochondrial ClO^- during ferroptosis.

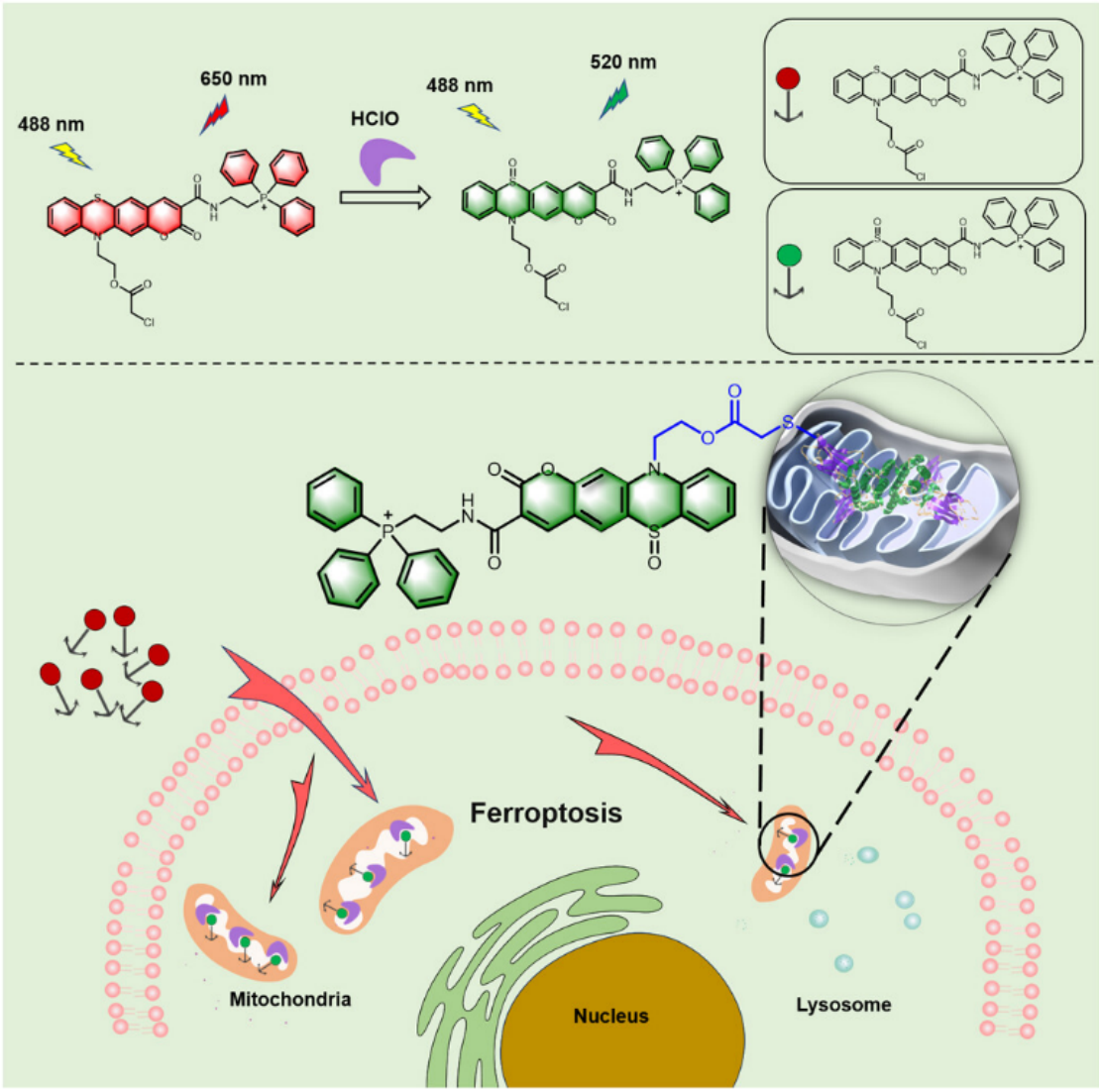

Figure 7. Proposed working principle for probe **YM-P**. Reproduced with permission [24]. Copyright 2025, American Chemical Society.

A series of D-π-A structures were synthesized by Cai et al. to screen fluorescent probes for the detection of ClO^- (Figure 8) [25]. The structure of 2-(3-cyano-4,5,5-trimethylfuran-2(5H)-ylidene)malononitrile (**TCF**) was selected as the acceptor. By using carbon-carbon double bond as the linker, **TCF** was connected to different electron-donating groups such as aniline, diphenylamine, and triphenylamine. As the electron-donating ability decreased, the Stokes shift of the probe, the electrophilic activity of the recognition site, and the spectral shift before and after reaction with ClO^- gradually increased. The maximum Stokes shift could reach 201 nm, and the probes exhibited three response modes: fluorescence quenching, ratiometric fluorescence, and fluorescence turn-on. These probes all had low detection limits (37.0, 5.1, and 1.0 nM respectively) and shown excellent selectivity in the presence of 16 different interfering substances. By combining three probes into a fluorescent sensor array, trace ClO^- could be quantitatively detected on-site. Based on this, it was proven that modulating the electron-donating strength of the donor group was a new strategy for designing reactive oxygen species probes.

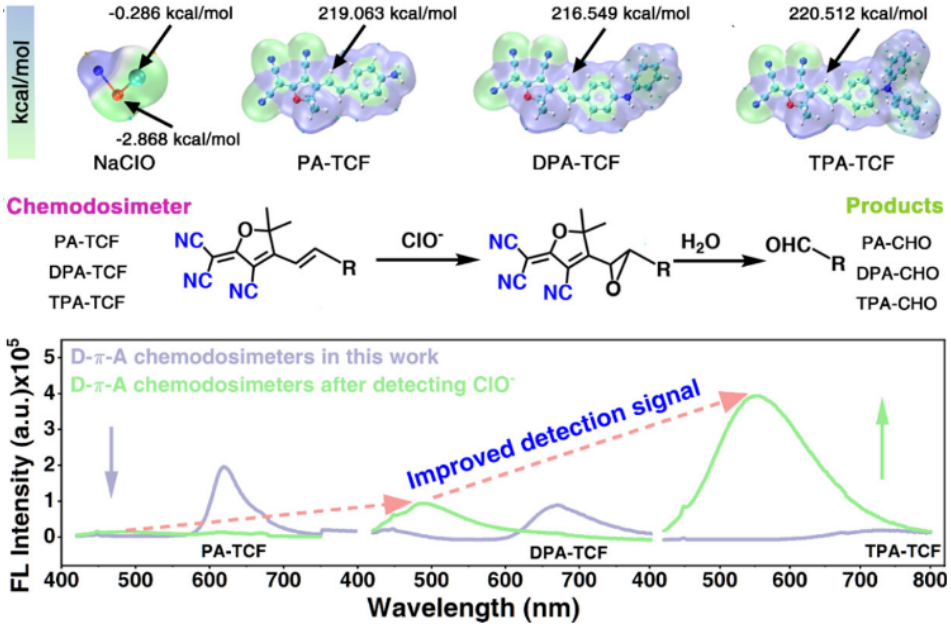

Figure 8. Proposed mechanism for **TCF** probes. Reproduced with permission [25]. Copyright 2025, American Chemical Society.

Small organic molecule-based sensors can further be incorporated with nanomaterial to enhance the sensing abilities. For example, Li et al. used Er^{3+} ion-doped nanoparticles as a reference and an elastomeric dye molecule (Cy925) as a ClO^- recognition site, which were combined with an amphiphilic polymer to form a water-soluble ratio nano-probe (Figure 9) [26]. Upon the addition of ClO^-, the conjugated structure of Cy925 was disrupted and a non-fluorescent structure was formed, leading to a weakening of its near-infrared fluorescence and thus a change in the ratio value. The sensitivity and high selectivity of the nanoprobe to ClO^- were verified by photoluminescence titration and selectivity experimental tests. Subsequently, the authors performed the determination of endogenous ClO^- in living mice and found that the ratio probe was suitable for tracking the change of ClO^- concentration in model mice with acute inflammation over a certain period of time.

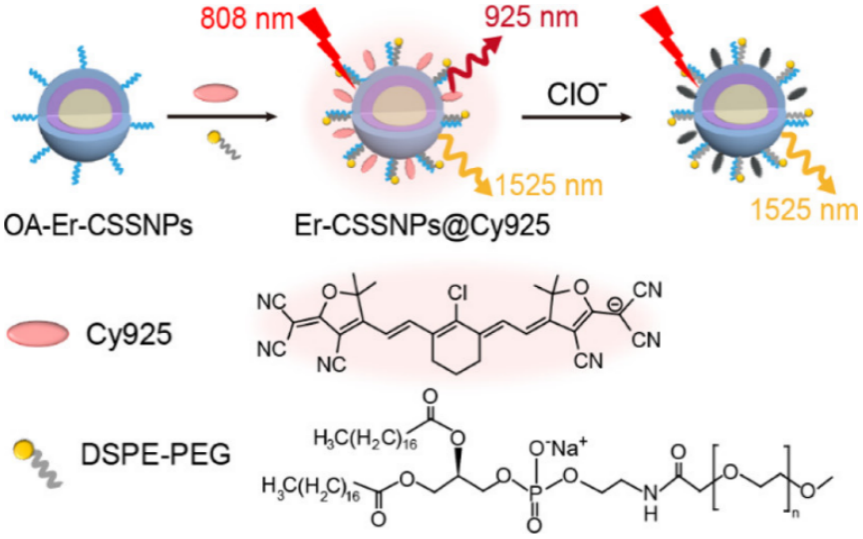

Figure 9. Design and testing of fluorescent probes for Er-CSSNPs@Cy925 ClO^-. Reproduced with permission [26]. Copyright 2019, American Chemical Society.

In some cases, the strong oxidative activity of ClO^- could lead to decomposition of the sensor structure, which is meaningful to change the emission properties of the solution. In this respect, Wang et al. designed and synthesized a novel fluorescent probe **EDPC** on the basis of coumarin and 4-dimethylaminobenzaldehyde for the detection of ClO^- with a low detection limit of 1.2×10^{-8} M in Tris-HCl buffer (pH = 7.2, 10 mM, containing 50% ethanol, Figure 10) [27]. Due to the oxidation reaction between C-O of coumarin lactone and C=C formed by condensation of hydroxyl aldehyde, **EDPC** has high selectivity and sensitivity for ClO^-. Moreover, in practical

applications, good recoveries ranging from 99.7% to 106.5% were obtained by **EDPC** testing of real water samples. In addition, the **EDPC** probe shows very low cytotoxicity and can be used for imaging exogenous and endogenous ClO^- in live HEK293 cells.

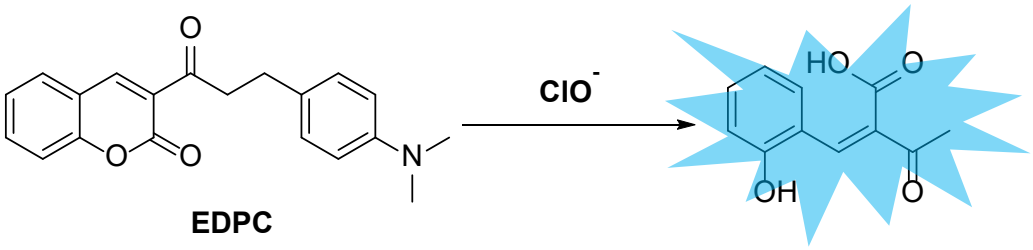

Figure 10. Design and Testing of Fluorescent Probes for **EDPC** ClO^-.

Looking through these results, we could summary that these probes primarily operate through two strategies: deprotection of masking groups or oxidation of specific elements. Since a sensitivity of 0.23 nM has been achieved (probe **BPH**), we believe each step forward on the sensitivity and response speed would enable precise biological applications of the probe, such as real-time imaging of ClO^- in disease models and offering valuable insights for diagnosing and understanding oxidative stress-related conditions.

3. Fluorescent Probes for $ONOO^-$

$ONOO^-$ is a key signaling molecule and a potent mediator of oxidative stress and cellular damage. As a highly reactive nitrogen species formed by reaction of superoxide and nitric oxide, $ONOO^-$ is related to numerous diseases including neurodegenerative disorders, cardiovascular dysfunction, chronic inflammation, and cancer. Accurate detection of $ONOO^-$ is essential for understanding its biological functions, deciphering the mechanisms of oxidative stress-related pathologies, and developing targeted therapeutic strategies to mitigate its detrimental effects while preserving its beneficial signaling roles.

Ye et al. developed a selective fluorescent probe named **TFMU-SO_2D** for $ONOO^-$ (Figure 11) [28]. In the probe design, the authors selected 7-hydroxy-4-(trifluoromethyl)coumarin (TFMU) containing a sulfonate group as the fluorescent moiety and arylboronate as the recognition group for $ONOO^-$. When $ONOO^-$ was added, the arylboronic acid unit is cleaved, releasing sulfur dioxide (SO_2). Interestingly, SO_2 can consume a portion of the intracellular glutathione (GSH), thereby maintaining intracellular redox homeostasis and avoiding the inhibition of ferroptosis due to the loss of ROS during the recognition process. Fluorescence spectroscopy analysis showed that the presence of $ONOO^-$ induced a fluorescence enhancement phenomenon and the response signal showed a good linear relationship with the concentration of $ONOO^-$. In addition, **TFMU-SO_2D** can be applied for sensing of $ONOO^-$ in cellular environments.

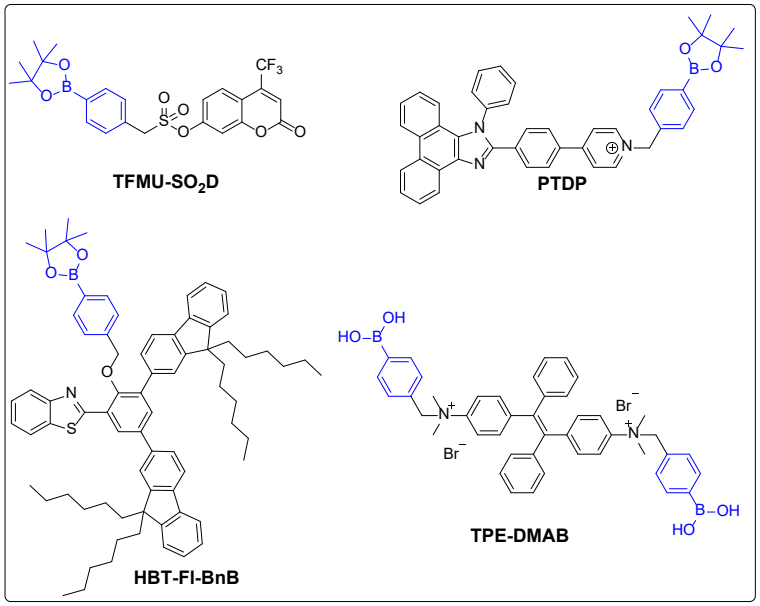

Figure 11. Chemical structure of probes TFMU-SO_2D, PTDP, HBT-Fl-BnB and TPE-DMAB.

Using benzeneboronic acid pinacol ester as the recognition unit, Mahapatra et al. reported a fluorescent probe named **PTDP** for specifically recognizing $ONOO^-$ (Figure 11) [29]. Optical studies demonstrated that **PTDP** exhibited high selectivity for $ONOO^-$. The sensing process was unaffected by other reactive oxygen species (ROS) and reactive nitrogen species (RNS). Probe **PTDP** possesses an intramolecular charge transfer (ICT) effect, displaying yellow fluorescence in solution. Upon the addition of $ONOO^-$, the probe undergoes a transformation that removes the phenylmethylboronic acid pinacol ester, reverting to the PPI and emitting blue fluorescence. This finding confirmed that **PTDP** is an effective ratiometric fluorescent probe for $ONOO^-$. Additionally, **PTDP** demonstrated excellent performance in live cell tests, indicating its potential for in vivo applications.

Yu et al. synthesized a ratiometric fluorescent probe, **HBT-Fl-BnB**, featuring zwitterionic ESIPT process for the detection of $ONOO^-$ with a LOD of 2.1 μM (Figure 11) [30]. The researchers introduced two fluorenyl (Fl) groups at the ortho and para positions of -OH in HBT, thereby transforming the original π-delocalized ESIPT characteristics. This modification enables the probe molecule to adopt a zwitterionic structure in the excited state, resulting in longer-wavelength fluorescence emission. Experimental results demonstrated that compared to analogs without the Fl groups, **HBT-Fl-BnB** exhibited superior fluorescence emission intensity and wavelength. Additionally, a boronic acid pinacol ester was incorporated to block the ESIPT effect, which can be removed in the presence of $ONOO^-$. **HBT-Fl-BnB** was successfully applied for imaging of both endogenous and exogenous $ONOO^-$ in living cells.

Tang et al. designed and synthesized an AIE-active fluorescent probe **TPE-DMAB** for simple and specific detection of $ONOO^-$ (Figure 11) [31]. The fluorescent probe contains a 4-(bromomethyl)phenylboronic acid as the recognition site for $ONOO^-$, which was attached to the AIEgen. The fluorescent probe **TPE-DMAB** showed fluorescence enhancement of up to 100-fold upon $ONOO^-$ induced cleavage of the phenylboronic acid moiety. The fluorescence intensity showed a good linear response with $ONOO^-$ concentration in a range of 3~12 mM, with a limit of detection of 54 nM. In addition, the fluorescent probe **TPE-DMAB** was highly selective for $ONOO^-$ over other tested ROS.

Kim et al. developed a new recognition site for $ONOO^-$, saying the diaminonaphthalene boronic acid (DANBA) (Figure 12) [32]. Traditional probes based on boronic acid or boronic ester were always interfered with by H_2O_2 during the measurement. In contrast, under protection of the diaminonaphthalene moiety, DANBA functionalized sensors showed significantly higher selectivity for $ONOO^-$ over H_2O_2. To verify this idea, the authors synthesized three pairs of different probes by incorporating three different fluorophores. The alkoxy group in the probes reacted with $ONOO^-$ to form a strong electron-donating hydroxyl group, thereby enhancing ICT effect and resulting in enhanced fluorescence emission. The experimental results demonstrated that the probes with DANBA as the recognition site exhibited higher sensitivity and selectivity towards $ONOO^-$ than that of the traditional boronic ester unit.

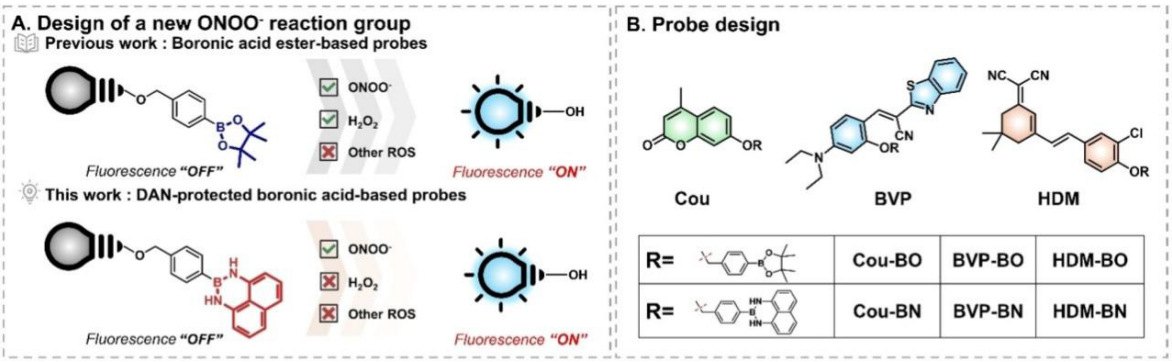

Figure 12. (**A**) Design principle for the **DANBA**-based probes; (**B**) Structural design of three pairs of different probes. Reproduced with permission [32]. Copyright 2024, John Wiley & Sons.

He et al. synthesized a ratiometric fluorescent probe named **NA-DP**, for tracking $ONOO^-$ and oxidative stress-induced mitophagy in live cells (Figure 13) [33]. The probe integrated a mitochondria-targeting triphenylphosphonium group and an $ONOO^-$ responsive diphenyl phosphinate moiety into a naphthalimide-based scaffold. The probe initially emitted fluorescence at 450 nm. Upon the addition of $ONOO^-$, the diphenyl phosphinate was converted into a hydroxyl group, which enhanced the ICT effect and led to a red-shift of the fluorescence emission to 550 nm. It exhibited high selectivity and sensitivity towards $ONOO^-$, with a detection limit of 0.31 μM. **NA-DP** successfully visualized $ONOO^-$ in live cells under oxidative stress conditions and distinguished oxidative stress-induced mitophagy from starvation-induced mitophagy, which is independent of $ONOO^-$.

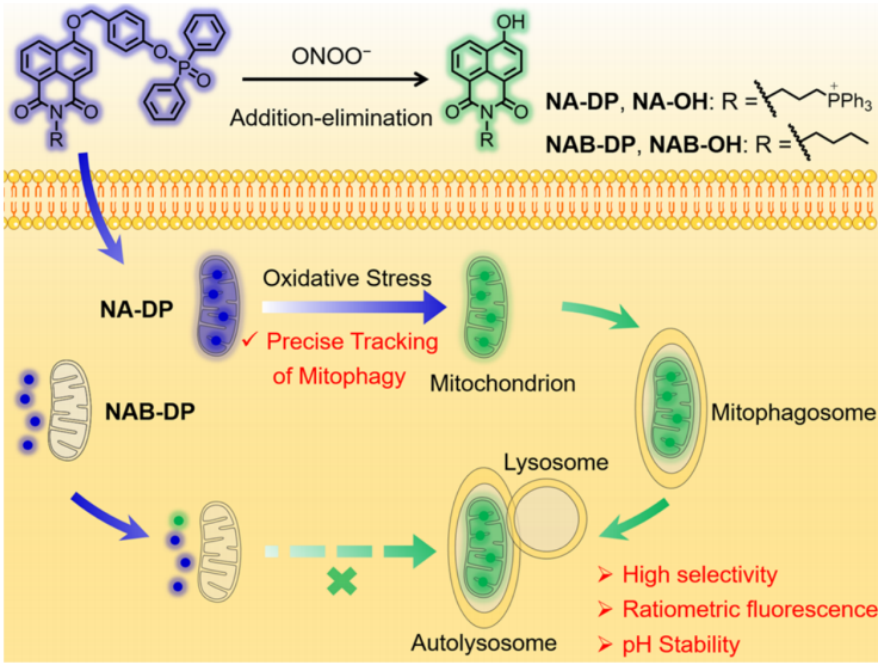

Figure 13. Sensing mechanism of **NA-DP** for the oxidative stress-induced mitophagy. Reproduced with permission [33]. Copyright 2024, American Chemical Society.

Kim et al. designed a fluorescent probe, **Mt-NI-2**, for detecting $ONOO^-$ in human serum and $ONOO^-$ imaging in living cells (Figure 14) [34]. 1,8-Naphthalimide was chosen as the fluorophore, modified with a triphenylphosphonium cation to enhance its mitochondrial targeting ability. The hydrazone bond served as the recognition group, which facilitated ICT effect and quenched the fluorescence. Upon the addition of $ONOO^-$, the hydrazone bond was converted to an aldehyde, inhibiting ICT effect within the system and causing the probe to emit fluorescence at 450 nm. The detection limit was calculated to be 6.5 nM. The probe was successfully applied for the evaluation of $ONOO^-$ levels in the mitochondria and serum of patients with Parkinson's disease.

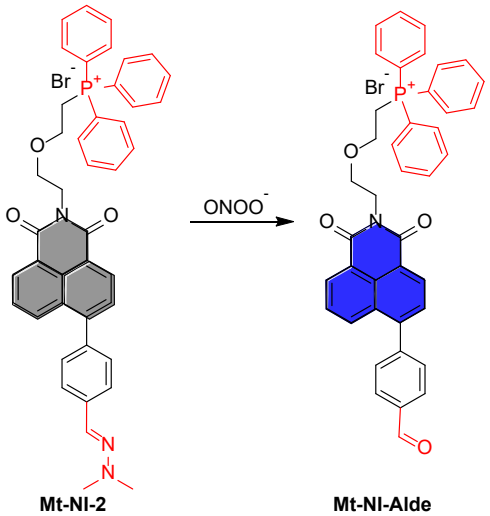

Figure 14. Proposed working principle for **Mt-NI-2**.

Yuan et al. reported a Ru complex **Ru-BCB** based on the luminescence resonance energy transfer (LRET) mechanism for the detection of $ONOO^-$ (Figure 15) [35]. Two amide bonds were used to connect the Ru(II) complex with 4-(2-carboxyphenyl)-7-diethylamino-2-(7-diethylamino-2-oxochroman-3-yl)-chromylium perchlorate (BCB). The emission spectrum of the Ru(II) complex effectively overlapped with the absorption spectrum of the BCB fluorophore, which facilitated LRET. Before the reaction, **Ru-BCB** transferred energy to BCB through the LRET mechanism, emitting NIR fluorescence at 700 nm. The electron-deficient benzopyran acted as a recognition group. After interaction with $ONOO^-$, the BCB part was oxidized and decomposed, and the LRET disappeared. The Ru (II) complex then emitted red luminescence at 632 nm, while the newly formed fluorophore 7-diethylamino-3-carboxy-

4-methylcoumarin (BC) emitted blue fluorescence at 471 nm. All three-luminescence signals show good linear relationships with the addition of $ONOO^-$, allowing for quantitative detection of $ONOO^-$. More importantly, in multi-channel mode, any two channels can be used for the ratiometric detection of $ONOO^-$.

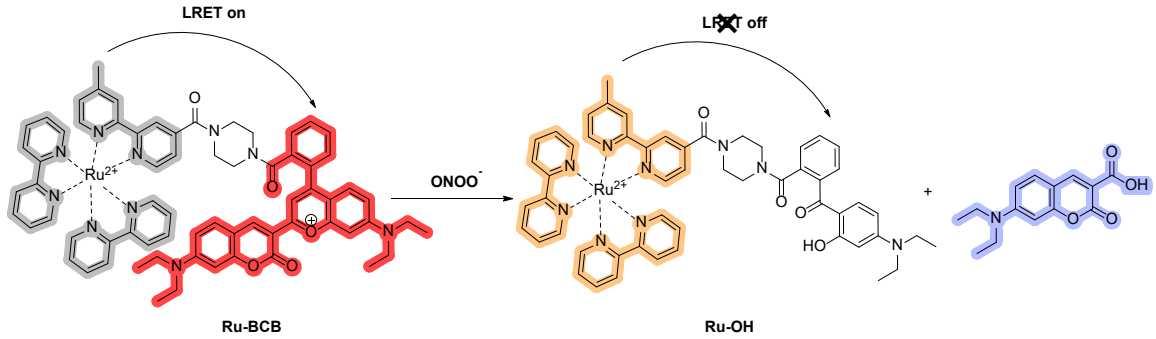

Figure 15. Proposed $ONOO^-$ sensing mechanism of probe **Ru-BCB**.

To achieve a larger Stokes shift and a longer emission wavelength, Wang et al. reported a fluorescent probe named **Rd-DPA3** for the detection of $ONOO^-$ (Figure 16) [36]. In the chemical structure of **Rd-DPA3**, rhodol fluorophore was expanded with a 1,4-diethylpiperazine moiety. The introduction of 4,4′-azobisphenol not only served as a recognition group but also endowed the probe with PET effect, thereby quenching the fluorescence. Upon the addition of $ONOO^-$, the bisphenol part was first oxidized to an alkylamine-modified fluorophore, which then underwent an elimination reaction to form **NIR-Rd-3**, emitting intense fluorescence at 700 nm, with a detection limit of 3.4 nM for $ONOO^-$. Using **NIR-Rd-3**, researchers realized real-time in vivo imaging of $ONOO^-$ concentration fluctuations in the brains of AD mice.

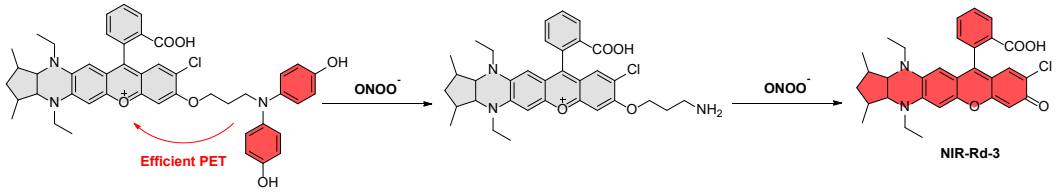

Figure 16. Proposed sensing mechanism for **Rd-DPA3**.

Mu et al. designed and synthesized **DHQM**, an endoplasmic reticulum-targeted AIE fluorescent probe, which exhibits high sensitivity and high selectivity for the detection of $ONOO^-$ under physiological conditions (Figure 17) [37]. The fluorescent probe used quinoline-malononitrile, a fluorophore with AIE characteristics, as the core backbone. N-aminophenol was integrated with the quinoline-malononitrile fluorophore as the $ONOO^-$ recognition site, and p-toluene-sulfonamide was introduced to give the probe specific endoplasmic reticulum-targeting ability. In addition, **DHQM** showed remarkable selectivity and extremely high sensitivity (detection limit of 97 nM) for $ONOO^-$ and exhibited specific anticancer activity, rapid response and wash-free intracellular imaging capability.

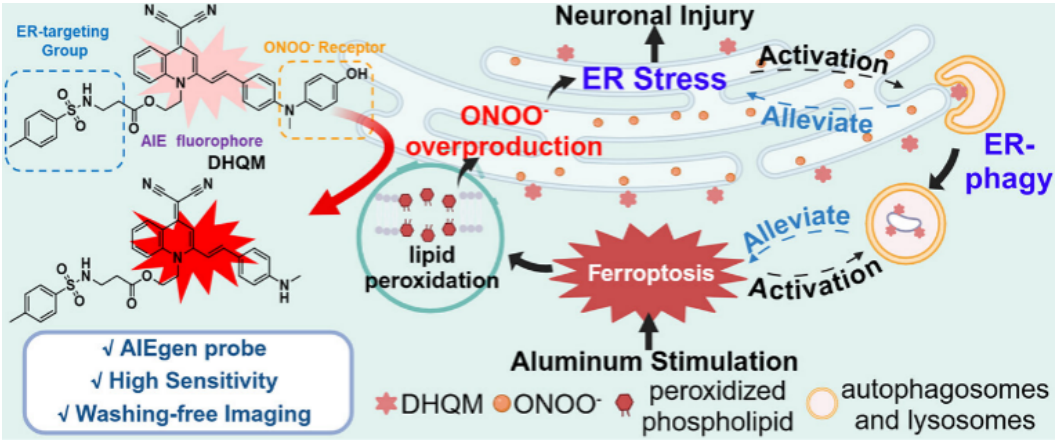

Figure 17. Proposed working principle for **DHQM**. Reproduced with permission [37]. Copyright 2025, American Chemical Society.

To reduce background fluorescence, Li et al. developed hydrogenation phosphorus-substituted rhodamine (**H-PRh**), which possesses "zero" background fluorescence due to the absence a conjugated structure (Figure 18) [38]. The probe demonstrated a linear response to $ONOO^-$ concentrations ranging from 0 to 40 μM, with a detection limit of as low as 18.9 nM, indicating its high sensitivity to $ONOO^-$. Kinetic studies confirmed the ultrafast response of **H-PRh** to $ONOO^-$. Additionally, the authors confirmed the probe's significant potential for both in vivo and in vitro applications through in vivo cell studies and the creation of a mouse model for hepatorenal syndrome.

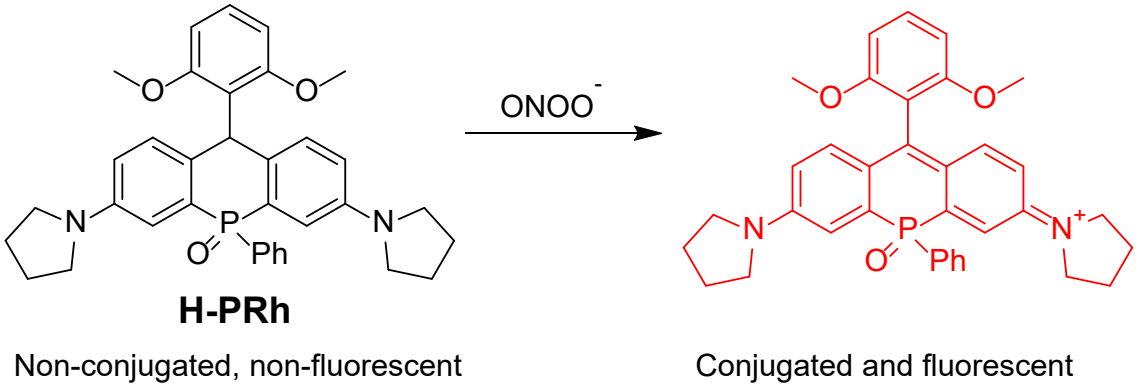

Figure 18. Recognition mechanism of **H-PRh**.

From these examples, we discovered that a dominant design strategy involves $ONOO^-$-specific cleavage of recognition units, particularly arylboronates, to trigger fluorescence signals via mechanisms like intramolecular charge transfer (ICT) or aggregation-induced emission (AIE). Some probes achieved remarkable sensitivity, selectivity and capabilities for ratiometric sensing and organelle-specific targeting. Looking forward, future efforts will likely focus on creating probes with even greater specificity to distinguish $ONOO^-$ from other oxidants in complex environments and extending emission wavelengths for deeper tissue imaging.

4. Detection of Other Oxidative Stress Species

Actually, oxidative stress could be induced by various reactive oxygen species and reactive nitrogen species. Recently, fluorescent probes for superoxide anion ($•O_2^-$), hydroxyl radical (•OH), and hydrogen peroxide (H_2O_2) have been reported. These oxidative species are also of paramount importance in both physiological and pathological systems since they are crucial signaling molecules and agents of oxidative stress. While H_2O_2 acts as a key secondary messenger in redox signaling pathways, its precursor $•O_2^-$ and the highly reactive •OH can cause severe damage to biomolecules. The precise detection and differentiation of these specific ROS are therefore critical for understanding the underlying mechanisms of numerous diseases.

Qian et al. reported an activable dual-optical molecular probe **CL-SA**, for imaging superoxide anion in epilepsy (Figure 19) [39]. The recognition mechanism of **CL-SA** relied on its chemiluminescent coelenterazine (CLA) unit, which was linked to a fluorescent dicyanoisophorone framework by a C=C bond. Upon interaction with $•O_2^-$, the CLA unit underwent oxidation to form a dioxetanone intermediate. This intermediate subsequently decomposed to generate a singlet-excited amide, which emitted chemiluminescence as it decayed to its ground state. Simultaneously, the reaction with $•O_2^-$ induced the opening of the oxoimidazole ring in the probe's structure, reducing its electron-withdrawing capacity and restoring the ICT effect. This restoration enhanced the fluorescence emission. The dual activation of chemiluminescence and fluorescence provided a highly sensitive (LOD = 54 nM) and selective response to $•O_2^-$, enabling the probe to effectively detect and image $•O_2^-$ in biological systems.

Jiang et al. designed a NIR fluorescence probe, **NIR-FP**, to monitor $•O_2^-$ fluctuations in ferroptosis-mediated epilepsy (Figure 20) [40]. The probe's precursor **FP-OH** featured a typical D-π-A structure, which exhibited strong ICT effect. By incorporating a highly electron-withdrawing triflate group, the ICT effect of the probe was interrupted, resulting in fluorescence quenching. The triflate group also acted as a recognition site for $•O_2^-$. Upon nucleophilic attacked by $•O_2^-$, the triflate was displaced, thereby restoring the probe's fluorescence. The probe demonstrated high sensitivity and selectivity for $•O_2^-$ detection, with a detection limit of 53 nM and an emission wavelength of 650 nm. It was successfully applied to image $•O_2^-$ in various ferroptosis-mediated epilepsy models.

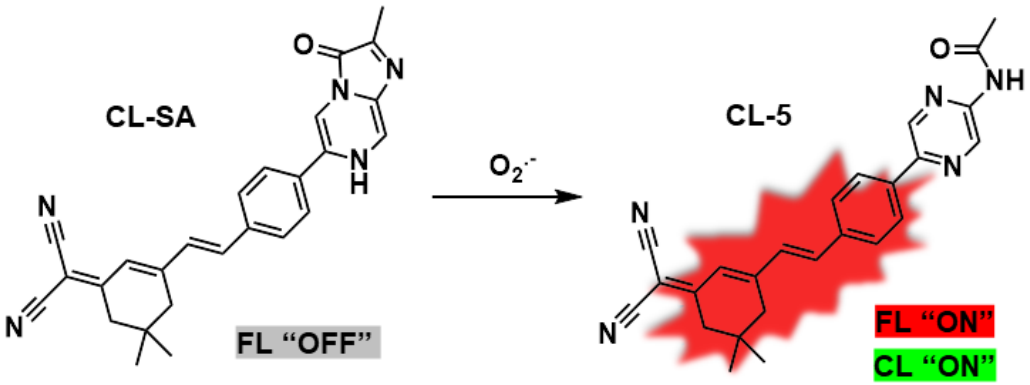

Figure 19. Proposed sensing mechanism for **CL-SA**. Reproduced with permission [39]. Copyright 2024, American Chemical Society.

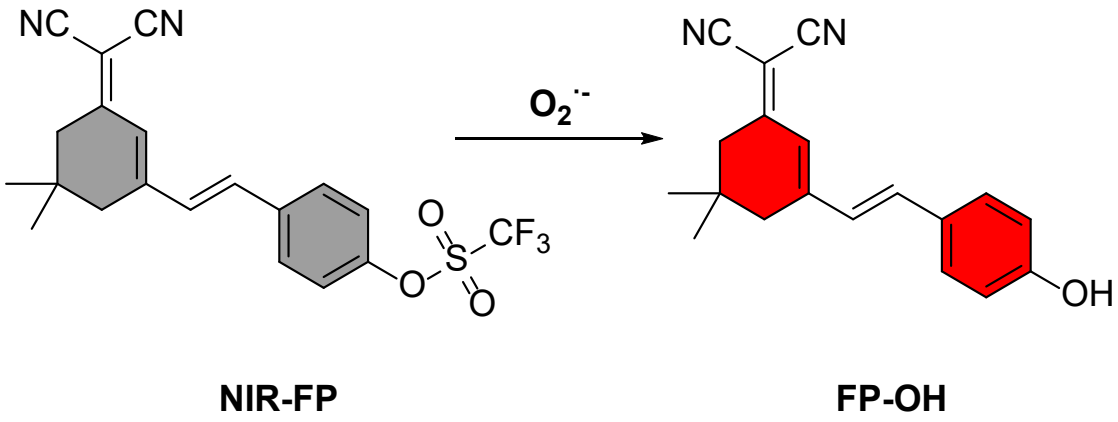

Figure 20. Chemical structure of **NIR-FP** and its sensing mechanism.

Previous studies have found that edaravone can act as a hydroxyl radical eliminator, generating stable 2-oxo-3-(phenylhydrazono)-butanoic acid (**OPB**) via free radical intermediates. Therefore, the edaravone structure was introduced to rhodamine fluorophore by Yang et al. to prepare a probe molecule **RH-EDA** (Figure 21) [41]. Due to the twisted ICT phenomenon, the probe molecule is non-fluorescent by itself. When •OH is added, the recognition group was converted to an **OPB** derivative, generating an enhanced fluorescence for specific recognition of •OH. The authors verified that the probe can be used to detect endogenous •OH in live cells and zebrafish model.

Yuan et al. developed a dual-site fluorescent probe **ZY-5** for simultaneous and independent monitoring of changes in polarity and •OH during ferroptosis (Figure 22) [42]. The probe was designed with a piperazine ring as the central linker, connecting a •OH responsive site and a polarity-sensitive unit. The •OH recognition site, which is based on a hydrocyanine moiety, underwent hydrogen abstraction by •OH, resulting in an expanded π-conjugation system. This alteration triggered a Förster Resonance Energy Transfer (FRET) effect, leading to red fluorescence emission at 637 nm. The detection limit for •OH was found to be 0.262 μM. Conversely, on the opposite side of the piperazine ring, a D-π-A triphenylamine unit was designed to detect changes in polarity. This unit displayed strong blue fluorescence emission at 426 nm in low-polarity environments due to the Intramolecular Charge Transfer (ICT) effect. The optimized molecular structure of **ZY-5** minimized spectral overlap between the two channels, allowing for independent and efficient detection of •OH and polarity changes in biological systems.

Li et al. designed a sensitive fluorescence probe **Cy7-1** for •OH (Figure 23) [43]. The probe was based on the cyanine dye Cy7, with a methoxy group substituted at the central phenyl ring as the recognition unit for •OH. Upon reaction with •OH, the phenol formed rapidly underwent a deprotonation reaction, leading to rearrangement of a larger polymethine π-conjugated system. This caused a red shift in the fluorescence signal that even reached the NIR region, thereby enabling highly sensitive detection of •OH. Using this probe, researchers have successfully studied the generation of trace amounts of •OH in physiological and pathological processes related to iron autoxidation.

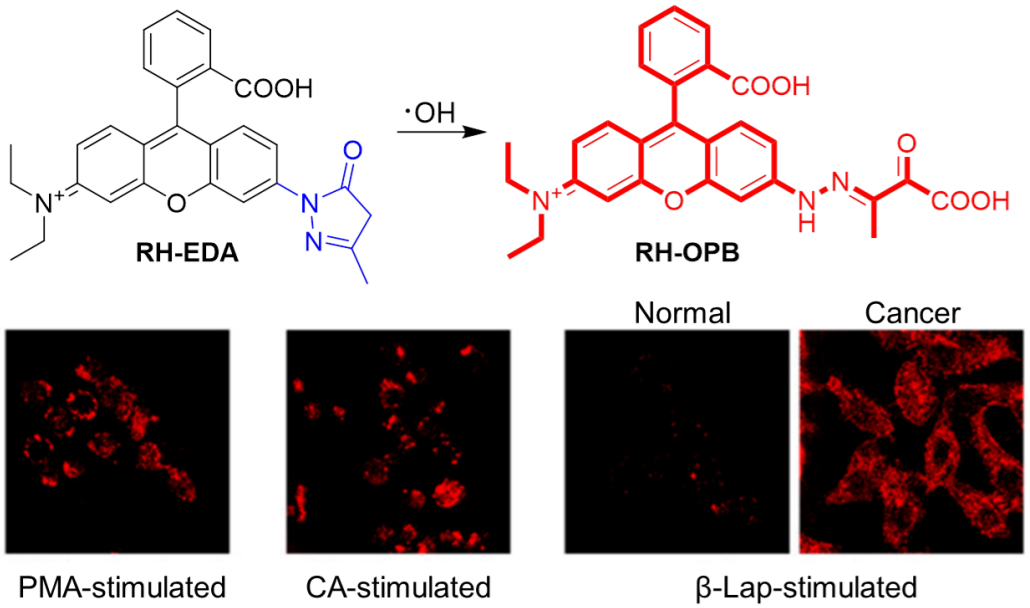

Figure 21. Proposed working mechanism for the **RH-EDA**. Reproduced with permission [41]. Copyright 2021, American Chemical Society.

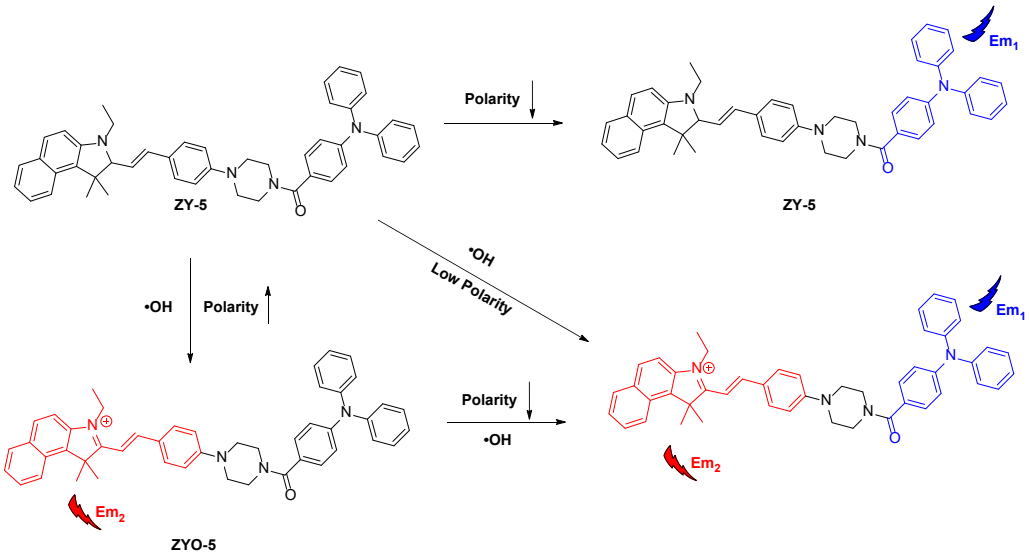

Figure 22. Proposed working principle of probe **ZY-5**.

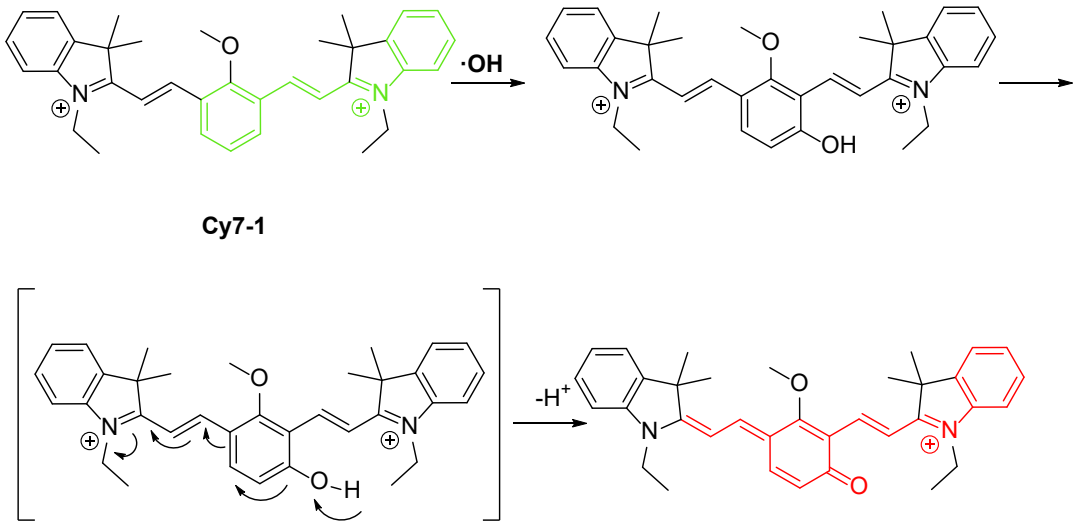

Figure 23. Proposed •OH sensing mechanism for **Cy7-1**.

Kim et al. developed a molecular fluorescent proportional response probe (**NPDIN**) for detecting H_2O_2 levels in COX-2 cancer cells, whose structure consists of indomethacin (COX-2 inhibitor) coupled with 1,8-naphthylphthalimide borate (Figure 24a) [44]. It was demonstrated that the indomethacin component of **NPDIN** possesses the ability to target COX-2 positive cancer cells. Moreover, it was verified that the probe **NPDIN** has high specificity and sensitivity for H_2O_2 over other interfering analytes such as $•O_2^-$, tert-butyl radical, tert-butyl peroxide, ClO^-, •OH and $ONOO^-$.

Long et al. reported a NIR-II fluorescent probe, **CT-XA-H_2O_2**, for tracking oxidative stress in plant sprouts caused by heavy-metal ion contamination or high-level salt exposure (Figure 24b) [45]. The probe leverages the intrinsic fluorescence properties of cyano-thiazole as an electron-accepting moiety and xanthane-aminodiphenyl as an electron-donating moiety, with dioxaborolane serving as a biomarker-responsive unit and fluorescence quencher. Upon encountering H_2O_2, the dioxaborolane is cleaved, leading to the formation of the dye **CT-XA-OH**, which exhibits significant fluorescent signals for detecting and imaging in H_2O_2 Notably, the aminodiphenyl group endows the chromophore with AIE characteristics, enhancing fluorescence in the aggregated state within an aqueous environment.

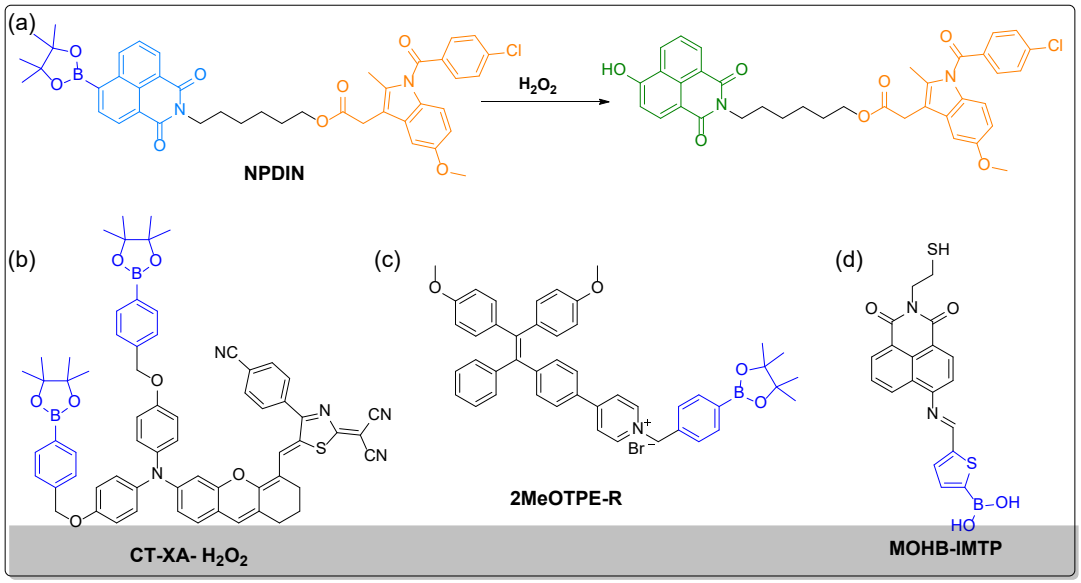

Figure 24. (**a**) Chemical structure of probe **NPDIN** and its H_2O_2 sensing mechanism; (**b**) Chemical structure of probe **CT-XA-H_2O_2**; (**c**) Chemical structure of probe **2MeOTPE-R**; (**d**) Chemical structure of probe **MOHB-IMTP**.

Zhang et al. established a new fluorescent probe using aggregation-induced emission (AIE) of tetraphenylstyrene units and the reaction of H_2O_2 with arylboronate groups, and successfully applied it for selective detection of H_2O_2 and D-glucose (Figure 24c) [46]. The underlying principle is that H_2O_2 oxidizes the phenyl borate ester component of **2MeOTPE-R** to form a phenol group. This process, followed by hydrolysis and 1,6-elimination of hydroquinone methyl ether, leverages the AIE properties of TPEs, resulting in low solubility in aqueous solutions. Consequently, the compound aggregates, leading to the activation of fluorescence in the TPE portion. Additionally, by integrating an another enzymatic reaction (oxidation of D-glucose by glucose oxidase to produce H_2O_2), **2MeOTPE-R** was further applied to selectively detect D-glucose in aqueous environments. Furthermore, the fluorescent probe demonstrates excellent sensitivity and selectivity for H_2O_2, with a detection limit of 180.0 nM, and for D-glucose, detectable at concentrations as low as 3.0 μM.

Dou et al. synthesized a series of naphthalimide-based fluorescent probes with precisely modulated π-conjugated bridges for detecting H_2O_2 (Figure 24d) [47]. By incorporating thiophene, benzene, and furan as π-bridge units between a boric acid recognition unit and a naphthalimide fluorophore, they constructed probes with distinct sensing capabilities. Among them, probe **MOHB-IMTP**, featuring a thiophene π-bridge, exhibited superior performance with a remarkable fluorescence response to H_2O_2 with a LOD of 38.5 nM. Furthermore, by integrating cellulose into probe, **MOHB-IMTP**/cellulose probe achieved an enhanced detection limit of 4.0 nM and was successfully applied in a portable device for rapid and sensitive H_2O_2 detection. This work highlighted the importance of π-conjugated bridge modulation in designing high-performance fluorescent probes for practical applications.

In this section, the development of sophisticated fluorescent probes for $•O_2^-$, •OH and H_2O_2 are discussed. Utilizing specific reaction-based recognition mechanisms, these probes achieved high sensitivity and selectivity,

enabling the tracking of corresponding ROS in biological models of disease. The advancements highlight a growing capability of fluorescent probes to decipher complex oxidative signaling pathways.

5. Fluorescent Probes for Oxidative Stress Related Multiple Targets

Compared to single analyte sensing, the simultaneous detection of multiple targets related to oxidative stress provides a comprehensive picture of redox status. This can be ascribed to the complex nature of oxidative stress, which interconnected a network of oxidants, antioxidants, and damage biomarkers, who are dynamically interdependent. By evaluating multiple targets, researchers will be able to diagnose the severity of oxidative damage in a more accurate way.

As an example, probe **DHX-SP** was designed and synthesized by Tang et al. by utilizing dihydroxanthene as the parent fluorescent group, a trifluoromethanesulfonic acid group as the recognition element for $\bullet O_2^-$, and a phenylboronate unit as the recognition site for $ONOO^-$ (Figure 25) [10]. Fluorescence analysis revealed that upon the addition of $\bullet O_2^-$, the probe **DHX-SP** cleaves the trifluoromethanesulfonic acid moiety to yield the phenol-containing probe **DHX-P**, which emits red fluorescence. The authors noted that this process involves the release of an ICT effect. When **DHX-P** encounters $ONOO^-$, it reacts with the phenylboronate moiety, resulting in an intense green fluorescence emission. Conversely, if $ONOO^-$ is added first, **DHX-SP** will react to form **DHX-S**, which does not produce a fluorescence signal at that stage. However, when $\bullet O_2^-$ is subsequently introduced to **DHX-S**, a green fluorescence signal is emitted due to the retention of the ICT effect in probe **DHX-S**. Fluorescence titration study demonstrated that probe **DHX-SP** exhibited a strong linear response correlation with both $\bullet O_2^-$ and $ONOO^-$. Additionally, the application of probe **DHX-SP** for monitoring $\bullet O_2^-$ and $ONOO^-$ into ferroptosis of PC12 cells and in the PD model yielded promising results.

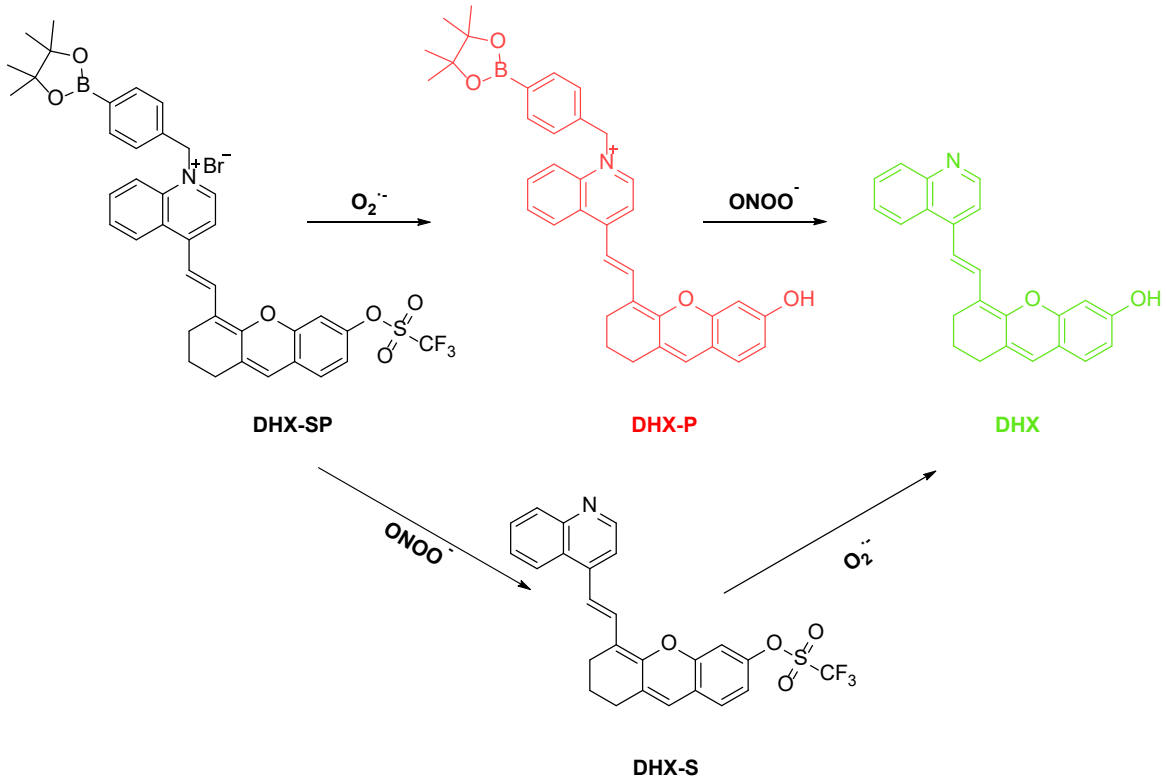

Figure 25. Proposed $O_2^{\bullet-}$ and $ONOO^-$ sensing mechanism for probe **DHX-SP**.

Zhao et al. synthesized a fluorescent probe **DBCC** which can selectively detect $^1O_2$ and ClO^- in lipid droplets (Figure 26) [48]. The probe selected Nile red as an LD localization dye, linking it to coumarin through an ester bond. In the design, both of $^1O_2$ and ClO^- possessed strong oxidizing properties and could attack the ester bond in **DBCC**, thereby releasing the coumarin molecule and restoring the fluorescence of the probe. Furthermore, compared to other ROS, ClO^- could open the lactone ring, thereby generating distinct fluorescence signals to differentiate $^1O_2$ from ClO^-. The probe has been successfully applied for the detection of exogenous and endogenous $^1O_2$ and ClO^- in HepG2 cells and zebrafish.

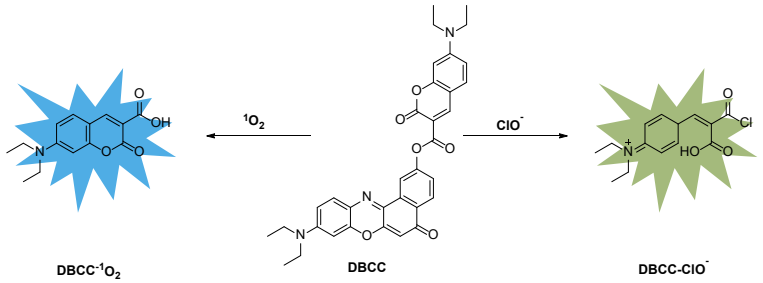

Figure 26. Schematic diagram of the reaction of probe **DBCC**.

Tang et al. designed a fluorescent probe, **NBO**, which could be used for continuous detection of $ONOO^-$ and HOBr in Alzheimer's disease (AD) model (Figure 27) [49]. The probe utilizes naphthalimide as the fluorophore, incorporating an amino group at the 3-position to function as the recognition group for HOBr. The probe was modified with 4-nitrobenzaldehyde to form an α-ketoamide unit for the recognition of $ONOO^-$. When the probe interacts with $ONOO^-$, the α-carbonyl group dissociates to produce **NB-ONOO**, a process that enhances the ICT effect, leading to a significant fluorescence emission at 550 nm. The detection limit was calculated to be 42.9 nM for $ONOO^-$. The subsequent reaction of the amino group with HOBr resulted in cyclization, which further extended the conjugated system and caused a red shift in fluorescence to 610 nm. The detection limit was calculated to be 147.7 nM for HOBr. Using this probe, the researchers successfully achieved real-time imaging of $ONOO^-$ and HOBr in AD models and assessed the therapeutic effects of AD drugs.

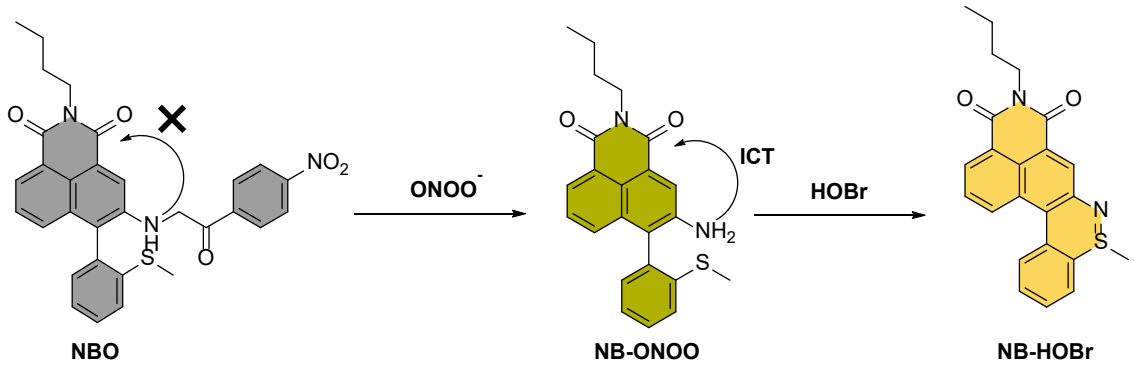

Figure 27. Proposed sensing mechanism of probe **NBO** for $ONOO^-$ and HOBr.

Lewis et al. designed and synthesized an effective two-photon fluorescent probe **AzuFluor 483-Bpin** for sensing of both $ONOO^-$ and H_2O_2 (Figure 28) [50]. This azulene-derived fluorescent probe is composed of an aboronate receptor moiety linked to an appropriately substituted azulene. This probe is photostable and possesses good cell penetration ability. It exhibits a higher selectivity for $ONOO^-$ over H_2O_2 without obvious cytotoxicity. Fluorescence titration experiments revealed that the detection limit of **AzuFluor 483-Bpin** for H_2O_2 was 1.72 μM, however, this fluorescent probe was much more sensitive to $ONOO^-$ than expected, with a detection limit of 21.7 nM determined by fluorescence titration experiments.

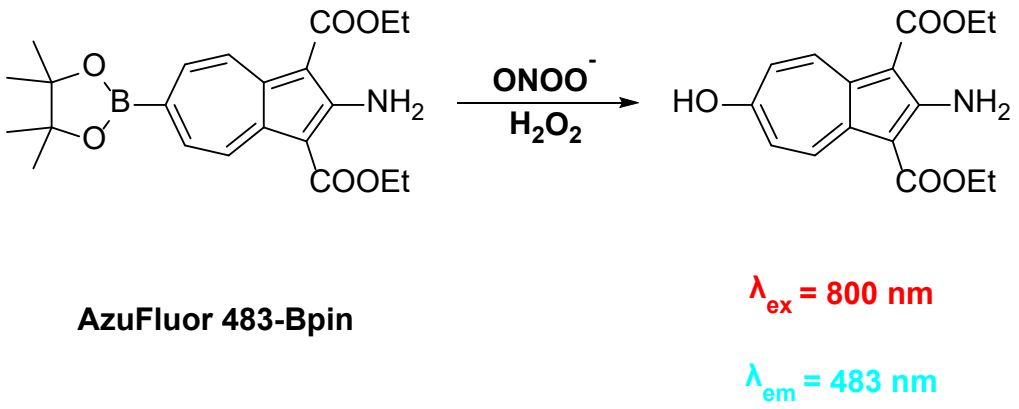

Figure 28. Proposed reaction mechanism of **AzuFluor 483-Bpin** with $ONOO^-$ and H_2O_2.

Song et al. reported a NIR probe **dfBDP** based on BODIPY for detecting F^- (LOD = 316.2 nM) and ClO^- (LOD = 33.9 nM) by different reaction mechanisms (Figure 29) [51]. P-tert-butyldimethylsilanolate benzyl thioether played the role as recognition unit. With the addition of F^-, the silicon-oxygen bond is cleaved, triggering a sequential elimination reaction, thereby removing the protection of -SH. This process strengthened the ICT effect, resulting in enhanced fluorescence emission at 940 nm. As a strong oxidizing agent, ClO^- can oxidize the thioether group in the probe, by oxidizing RS^- to sulfoxide. This conversion reduces the ICT effect, resulting in a blue shift in fluorescence emission to 575 nm. These mechanisms enabled **dfBDP** to specifically respond to F^- and ClO^-, and there was no overlap between the two response signals, providing the basis of detecting both species simultaneously.

Lee et al. introduced a dual-channel fluorescent probe **RATP-NClO**, which could synchronously detect ATP (LOD = 4.14 μM) and ClO^- (LOD = 0.1 μM) (Figure 30) [52]. The probe exhibits high selectivity and sensitivity for both targets. Upon oxidation by ClO^-, the thiomorpholine group in **RATP-NClO** was converted into the structure as **NClO**, which emits green fluorescence with an emission wavelength observed at 534 nm. This fluorescence enhancement was attributed to the attenuation of PET effect. Upon the addition of ATP, the probe forms a stable complex known as **RATP**, which emits red fluorescence at 587 nm.

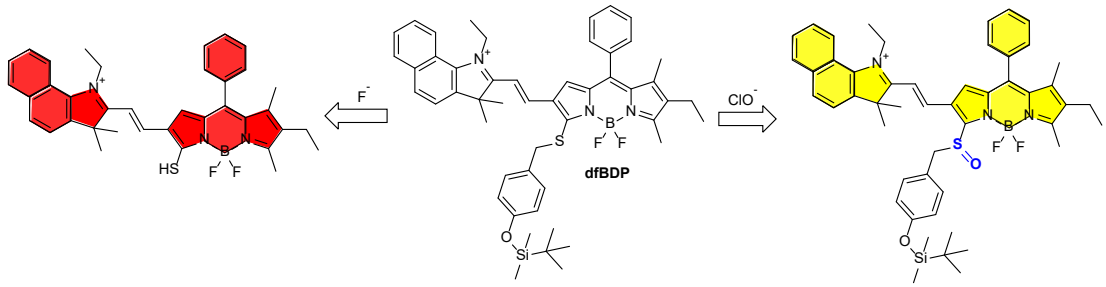

Figure 29. Design strategy of the probe **dfBDP** toward F^- and ClO^-.

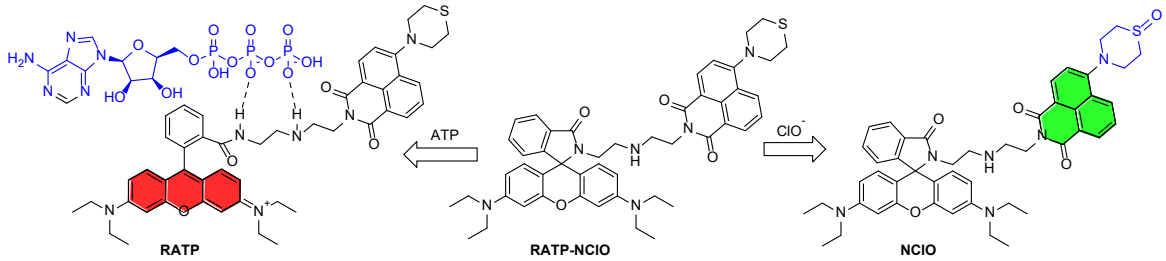

Figure 30. Proposed sensing mechanism for **RATP-NClO.**

Actually, oxidative stress of the living system is not only a result of over production of ROS and RNS. It also could be caused by abnormal produce of reducing substances such as GSH. Therefore, it is meaningful to design fluorescent probes for simultaneous detection of oxidative and reductive species in vivo. In this respect, Yuan et al. prepared an activable two-site fluorescent probe **OG-3** for sensing of both •OH and GSH (Figure 31) [53]. A hydrocyanine moiety with a large π-conjugation system was introduced on one side of the piperazine ring to act as a recognition site for •OH. The •OH can undergo the abstraction of a hydrogen atom from the hydrocyanine group. The reacted probe molecule shows red fluorescence due to the presence of FRET mechanism. The naphthalic anhydride unit containing dinitrobenzene sulfonate was introduced on the other side of the piperazine ring as a GSH recognition site. After reaction with GSH, the naphthylimide portion of the molecule shows green fluorescence through an ICT mechanism. The probe can be used to distinguish between •OH and GSH. The authors demonstrated by endogenous and exogenous assays that the probe can be used to monitor changes of GSH and •OH during iron death process in vivo.

Very recently, Liu et al. introduced a redox NIR fluorescent probe, **NIR-CSTe**, for monitoring the $ONOO^-$/GSH redox couple associated with ferroptosis and diabetes (Figure 32) [54]. The distinctive properties of tellurium, marked by its large atomic radius and low electronegativity, make tellurium-containing compounds more reactive toward oxidation compared to their sulfur analogs. In this study, researchers incorporated diphenyl telluride into the dihydroxanthene framework through Knoevenagel condensation reaction to synthesize **NIR-CSTe**. The probe's fluorescence was initially quenched due to the PET effect. When $ONOO^-$ was added, the oxidation of tellurium disrupted the PET effect, leading to a pronounced fluorescence enhancement. Subsequently, the addition of GSH restored the fluorescence to its original state, thereby achieving reversibility in the detection process.

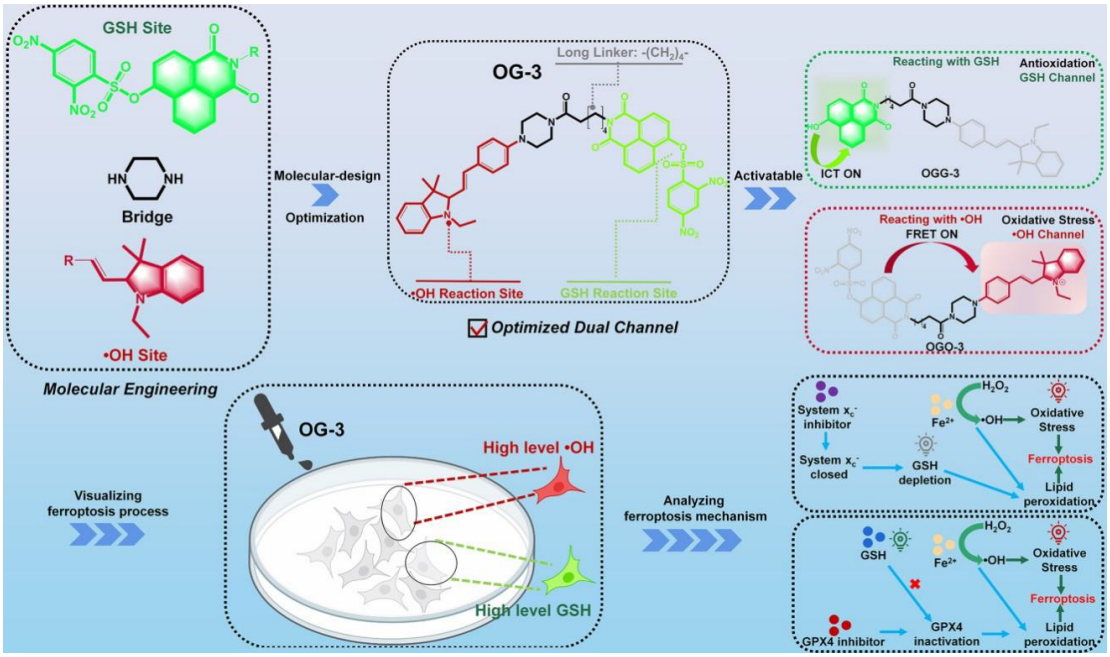

Figure 31. Recognition mechanism of **OG-3** for •OH and GSH. Reproduced with permission [53]. Copyright 2024, American Chemical Society.

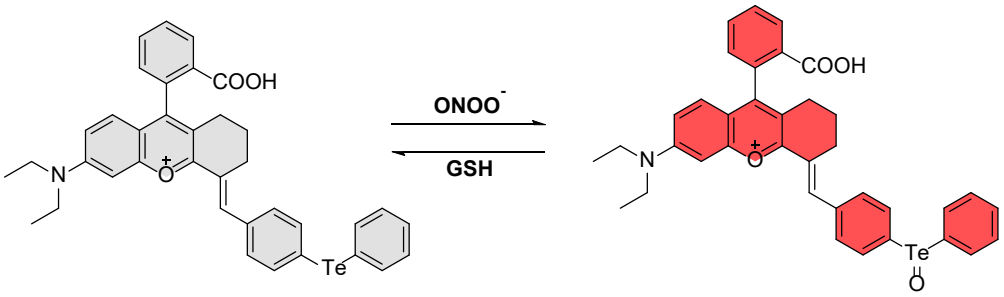

Figure 32. Proposed mechanism for **NIR-CSTe**.

The simultaneous detection of ROS and cell microenvironment is critically important because they are deeply intertwined in both physiological processes and the pathogenesis of numerous diseases. For example, ROS can directly influence cellular viscosity by damaging organelles. Conversely, the local viscosity of a cellular microenvironment profoundly affects the diffusion, lifetime, and reactivity of ROS. In this respect, Wang et al. introduced a hemicyanine-based fluorescent probe named **BDTB-PA**, designed for detecting ClO^- and viscosity (Figure 33) [55]. The probe leverages the principles of TICT, ESIPT, and AIE to achieve dual-response detection. In aqueous solutions, **BDTB-PA** exhibits low fluorescence background due to TICT, while the presence of ClO^- triggers the release of a hydroxyl group, activating ESIPT and AIE, resulting in a green emission at 540 nm (LOD = 13 nM). Conversely, in viscous environments, TICT is inhibited, leading to a red emission at 580 nm. The probe demonstrates high selectivity, rapid response, and low cytotoxicity, allowing for effective imaging of ClO^- and viscosity changes in living cells, plants, and zebrafish, offering a powerful tool for studying mitochondrial-related oxidative stress and dysfunction.

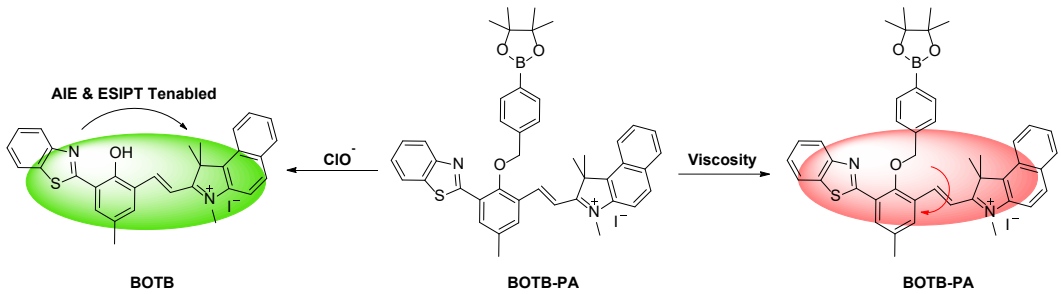

Figure 33. Proposed signal reporting mechanism of **BDTB-PA** toward ClO^- and viscosity.

Li et al. reported a dual-responsive NIR fluorescent probe **PBQI** (Figure 34) [56]. **PBQI** consists of a triphenylamine derivative with aggregation-induced emission (AIE) characteristics and a tetramethylquinoline derivative, linked by a vinyl group to form a D-π-A structure that enhances the intramolecular charge transfer effect. This design made the probe highly sensitive to changes in polarity with a strong red fluorescence emission developed at 700 nm when the polarity decreases. The propionic acid chain of the probe reacted with $ONOO^-$, resulting in a weakened PET effect and the release of the fluorophore, which emitted green fluorescence at 520 nm with a detection limit of 1.5 μM. **PBQI** filled the gap of probes for detecting $ONOO^-$ in low polar environments.

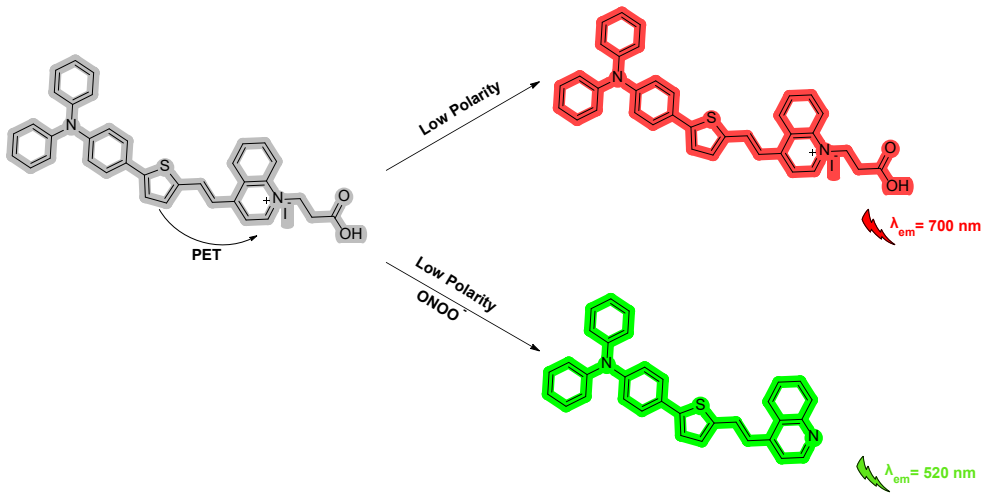

Figure 34. Proposed sensing mechanism for **PBQI**.

Shuang et al. reported a dual-channel fluorescent probe, **QX-DP**, for simultaneous detection of $ONOO^-$ and viscosity in disease models (Figure 35) [57]. Utilizing a xanthene unit as the electron donor, an ethylene group as the π-bridge, and a quinoline group as the electron acceptor, researchers constructed a probe precursor QX-OH with a D-π-A molecular structure. The diphenylphosphinate group, functioning as a recognition element, quenched the fluorescence of the probe. Upon the addition of $ONOO^-$, the diphenylphosphinate group underwent oxidative cleavage, restoring ICT effect and enhancing NIR fluorescence emission at 752 nm. The detection limit for $ONOO^-$ was found to be 127.4 nM. Using this probe, the elevated levels of $ONOO^-$ and viscosity in the brain tissues of epileptic mice were revealed, and the visual diagnosis of non-alcoholic fatty liver disease was achieved.

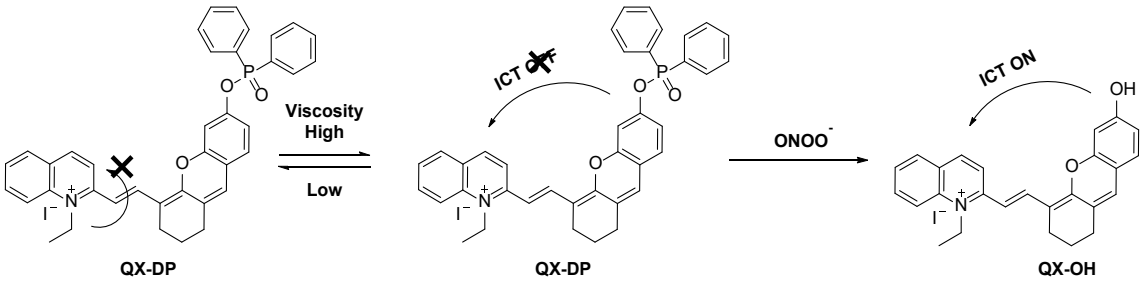

Figure 35. Proposed sensing mechanism for **QX-DP**.

Fu et al. developed a fluorescent probe, **WD-2**, which effectively monitored the levels of $ONOO^-$ and viscosity within lipid droplets and mitochondria during cell pyroptosis (Figure 36) [58]. This probe was designed with a naphthalimide dye as the fluorophore, incorporated long alkyl chains to enhance its targeting capability towards lipid droplets. The addition of $ONOO^-$ led to the oxidative cleavage of C=C bond between the naphthalene group and the indole group, resulting in the formation of NI-CHO, which emitted green fluorescence at 525 nm. **WD-2** demonstrated high sensitivity and selectivity for $ONOO^-$ detection, with a low detection limit of 28.79 nM, and showed excellent targeting ability towards both lipid droplets and mitochondria. It was successfully applied to track the dynamic changes of $ONOO^-$ levels in cellular and zebrafish, providing valuable insights into the role of $ONOO^-$ in the pathophysiological processes of cell pyroptosis.

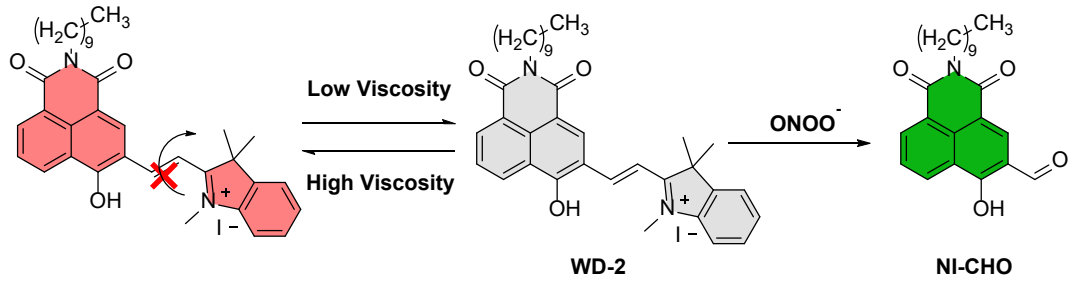

Figure 36. Proposed mechanism for **WD-2**.

Wang et al. synthesized a fluorescent probe, **HCy-BA**, for real-time monitoring of $ONOO^-$ and viscosity in cellular environments (Figure 37) [59]. The probe was designed using a D-π-A framework derived from hemicyanine, which incorporates a phenylboronic acid group as the receptor and an α-β unsaturated ester as the donor. In the presence of low concentrations of $ONOO^-$ (0–10 μM), the emission intensity of **HCy-BA** remained unchanged. However, upon exposed to higher concentrations of $ONOO^-$ (12–50 μM), **HCy-BA** exhibited strong fluorescence emission at 590 nm. This indicated that **HCy-BA** had the potential to differentiate between normal biological cells and cancer cells, which were typically characterized by elevated levels of $ONOO^-$. Moreover, the introduction of α-β unsaturated ester in **HCy-BA** effectively enhances the efficiency of intersystem crossing, thereby endowing the probe with the ability to generate $^1O_2$. This capability allowed **HCy-BA** to demonstrate significant photo-toxicity against tumor cells and effectively inhibit tumor growth in mice bearing tumors.

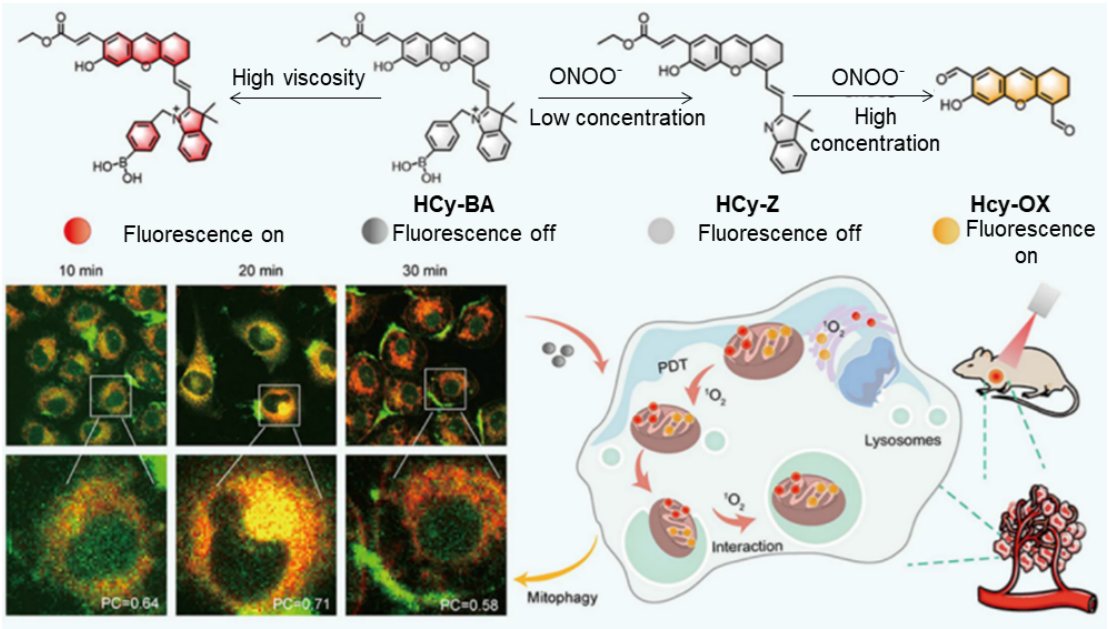

Figure 37. Application of probe **HCy-BA** for $ONOO^-$ and viscosity sensing in vivo. Reproduced with permission [59]. Copyright 2025, American Chemical Society.

As we can see, several multi-analyte fluorescent probes have been developed for simultaneous detection of reactive species such as $•O_2^-$/$ONOO^-$ or ClO^-/HOBr, and even redox couples like $ONOO^-$/GSH. By employing sophisticated sequential or orthogonal reaction mechanisms, these probes generate distinct fluorescent signals for each target, providing a dynamic and interconnected view of the redox landscape. This advanced capability allows researchers to accurately diagnose disease severity, elucidate complex pathological mechanisms, and evaluate therapeutic responses by capturing the intricate interplay between oxidants, antioxidants, and the cellular microenvironment.

6. Conclusions and Future Perspectives

In conclusion, significant progresses have been made in very recent years in the design of small organic molecule-based probes for measurement of oxidative stress. The probe structure, sensing mechanism and sensing performance are discussed with representative examples in detail. The detection limit and response time of some representative probes are summarized in Table 2. As demonstrated, a sensitive detection limit of 0.23 nM for ClO^-

was achieved using probe **BPH**, while probe **HBT-Fl-BnB** exhibited a rapid response time of 2 s for $ONOO^-$ detection. Looking into these recently reported achievements, we are confident of a bright future of using fluorescent probes as an analytical tool for oxidative stress. On the other hand, although research on the development of small organic molecule-based fluorescent probes for monitoring of oxidative stress has ongoing for about two decades, this is still a hot research topic. It can be ascribed to the challenges to design a practical fluorescent sensor for oxidative stress. Particularly, it is difficult to improve the selectivity when designing a probe for either ROS or RNS. In some cases, the selectivity could be even reversed as the same recognition unit could target different ROS/RNS analyte when it was incorporated in different fluorophores. Besides, relatively slow response speed or low reaction sensitivity is also an obstacle for practical application of the reported probes. As most of the fluorescent probes for detecting ROS/RNS are based on the breakage and formation of covalent bonds, it is difficult to accelerate the reaction speed especially in aqueous environment.

Table 2. Summary of representative fluorescent probes for oxidative stress.

Entries	Sensor's Name	Target	LOD	Response Time	Ref.
1	Cy-DM	ClO^-	0.84 μM	2 s	[15]
2	DL-Cl	ClO^-	0.32 μM	2.5 min	[17]
3	Pro-NBS	ClO^-	6 nM	3 min	[18]
4	SRF-ClO	ClO^-	2.7 nM	6 s	[19]
5	PNPM	ClO^-	15.3 nM	1 min	[20]
6	Nap-DCE	ClO^-	0.738 μM	3 s	[21]
7	BPH	ClO^-	0.23 nM	<10 s	[22]
8	GA-BOD-S	ClO^-	35 nM	13 s	[23]
9	HBT-Fl-BnB	$ONOO^-$	2.1 μM	2 s	[30]
10	TPE-DMAB	$ONOO^-$	54 nM	8 s	[31]
11	NA-DP	$ONOO^-$	0.31 μM	15 min	[33]
12	Mt-NI-2	$ONOO^-$	6.5 nM	1 min	[34]
13	Rd-DPA3	$ONOO^-$	3.4 nM	30 min	[36]
14	DHQM	$ONOO^-$	97 nM	<10 s	[37]
15	H-PRh	$ONOO^-$	18.9 nM	-	[38]
16	CL-SA	$\bullet O_2^-$	54 nM	<10 s	[39]
17	NIR-FP	$\bullet O_2^-$	53 nM	20 min	[40]
18	MOHB-IMTP	H_2O_2	4.0 nM	200 s	[47]
19	AzuFluor 483-Bpin	H_2O_2	1.72 μM	30 min	[50]
20	AzuFluor 483-Bpin	$ONOO^-$	21.7 nM	5 min	[50]
21	BDTB-PA	ClO^-	13 nM	30 s	[55]
22	PBQI	$ONOO^-$	1.5 μM	5 min	[56]
23	QX-DP	$ONOO^-$	127.4 nM	90 s	[57]
24	WD-2	$ONOO^-$	28.79 nM	10 min	[58]

Considering these facts, we propose that future research on the development of practical fluorescent probes for oxidative stress should be a systematic work. Since a lot of efforts have already been paid for designing a reasonable probe structures, the strategies to provide a suitable reaction microenvironment for the probe could be another breakthrough point. This could be learned from enzyme assisted reactions that occur in our body, which are selective, sensitive and efficient. Future work should focus on optimizing the reaction kinetics between the probe and ROS/RNS in biological media. Ultimately, these innovative fluorescent tools are not only illuminating fundamental biological processes but also paving the way for early diagnostic strategies.

Furthermore, the push towards multi-analyte detection presents both the greatssest challenge and the most promising opportunity. While probes that simultaneously monitor two or more species provide a more systems-level view of redox biology, their design is exponentially more complex. It requires meticulously orthogonal reaction mechanisms to prevent signal crosstalk and sophisticated molecular engineering to ensure distinct optical outputs. Future research on this subtopic should focus on developing novel reaction-based recognition sites with absolute specificity and creating reversible or reaction-ordered probes that can decode the sequence of oxidative events. Ultimately, overcoming these hurdles will unlock the potential to visualize the dynamic interplay within entire oxidative stress networks, moving beyond static snapshots to real-time functional analysis.

Funding

This work was supported by the National Natural Science Foundation of China (No. 22278229) and 333 High Level Talent Project of Jiangsu Province.

Institutional Review Board Statement

Not applicable.

Informed Consent Statement

Not applicable.

Data Availability Statement

This review article does not contain any new research data.

Conflicts of Interest

The authors declare no conflict of interest.

Use of AI and AI-Assisted Technologies

During the preparation of this work, the authors used OpenAI for language polishing. After using this service, the authors reviewed and edited the content as needed and take full responsibility for the content of the published article.

References

1. Pizzino, G.; Irrera, N.; Cucinotta, M.; et al. Oxidative Stress: Harms and Benefits for Human Health. *Oxidative Med. Cell. Longev.* **2017**, *2017*, 8416763. https://doi.org/10.1155/2017/8416763.
2. Chen, X.; Tian, X.; Shin, I.; et al. Fluorescent and luminescent probes for detection of reactive oxygen and nitrogen species. *Chem. Soc. Rev.* **2011**, *40*, 4783–4804. https://doi.org/10.1039/C1CS15037E.
3. Chen, X.; Wang, F.; Hyun, J.Y.; et al. Recent progress in the development of fluorescent, luminescent and colorimetric probes for detection of reactive oxygen and nitrogen species. *Chem. Soc. Rev.* **2016**, *45*, 2976–3016. https://doi.org/10.1039/C6CS00192K.
4. Sies, H.; Belousov, V.V.; Chandel, N.S.; et al. Defining roles of specific reactive oxygen species (ROS) in cell biology and physiology. *Nat. Rev. Mol. Cell Biol.* **2022**, *23*, 499–515. https://doi.org/10.1038/s41580-022-00456-z.
5. Cotruvo Jr, J.A.; Aron, A.T.; Ramos-Torres, K.M.; et al. Synthetic fluorescent probes for studying copper in biological systems. *Chem. Soc. Rev.* **2015**, *44*, 4400–4414. https://doi.org/10.1039/C4CS00346B.
6. Sedgwick, A.C.; Wu, L.; Han, H.-H.; et al. Excited-state intramolecular proton-transfer (ESIPT) based fluorescence sensors and imaging agents. *Chem. Soc. Rev.* **2018**, *47*, 8842–8880. https://doi.org/10.1039/C8CS00185E.
7. Wu, L.; Huang, C.; Emery, B.P.; et al. Forster resonance energy transfer (FRET)-based small-molecule sensors and imaging agents. *Chem. Soc. Rev.* **2020**, *49*, 5110–5139. https://doi.org/10.1039/c9cs00318e.
8. Lv, X.; Huang, W.; Jiang, N.; et al. A-D-A type fluorescent probe with dual quaternary-ammonium-salt anchors for turn on detection of HSA in wide emission gamut. *Spectrochim. Acta A* **2025**, *331*, 125772. https://doi.org/10.1016/j.saa.2025.125772.
9. Xu, S.; Yan, K.-C.; Xu, Z.-H.; et al. Fluorescent probes for targeting the Golgi apparatus: Design strategies and applications. *Chem. Soc. Rev.* **2024**, *53*, 7590–7631. https://doi.org/10.1039/D3CS00171G.
10. Xu, J.; Huang, H.; Wang, K.; et al. Design and Synthesis of BODIPY and Its Application in Inhibiting Intestinal Flora. *ACS Omega* **2024**, *9*, 44379–44384. https://doi.org/10.1021/acsomega.4c04882.
11. Bao, Y.; Lv, X.; Qu, Y.; et al. Red-Emissive Fluorescent Thermometer for Real-Time Monitoring of Intracellular and Architectural Glass Facade Temperature Variations. *ACS Sustain. Chem. Eng.* **2025**, *13*, 15627–15637. https://doi.org/10.1021/acssuschemeng.5c06460.
12. Gui, R.; Jin, H.; Bu, X.; et al. Recent advances in dual-emission ratiometric fluorescence probes for chemo/biosensing and bioimaging of biomarkers. *Coordin. Chem. Rev.* **2019**, *383*, 82–103. https://doi.org/10.1016/j.ccr.2019.01.004.
13. Xu, S.-L.; Guo, F.-F.; Xu, Z.-H.; et al. A hemicyanine-based fluorescent probe for ratiometric detection of ClO- and turn-on detection of viscosity and its imaging application in mitochondria of living cells and zebrafish. *Sens. Actuator B Chem.* **2023**, *383*, 133510. https://doi.org/10.1016/j.snb.2023.133510.
14. Mao, P.-D.; Liu, S.-S.; Lian, Z.-Y.; et al. Dual-channel fluorescent probe for monitoring the dynamic changes of hypochlorite ion and ATP in drug-induced liver injury. *Sens. Actuator B Chem.* **2025**, *440*, 137908.
15. Yang, K.; Tian, Y.; Zheng, B.; et al. Fast-Responsive HClO-Activated Near-Infrared Fluorescent Probe for In Vivo Diagnosis of Inflammatory Bowel Disease and Ex Vivo Optical Fecal Analysis. *Anal. Chem.* **2024**, *96*, 12065–12073. https://doi.org/10.1021/acs.analchem.4c02130.
16. Li, Z.; Huang, P.; Wu, G.; et al. Activatable Fluorescent Probe for Studying Drug-Induced Senescence *In Vitro* and *In Vivo*. *Anal. Chem.* **2024**, *96*, 12189–12196. https://doi.org/10.1021/acs.analchem.4c02423.

17. Zhao, G.; Wang, X.; Wen, M.; et al. Near-Infrared Fluorescence Reporter Offering Real-Time Tracking and Differential Assessment of Ferroptosis Progressions *In Vivo*. *Anal. Chem.* **2025**, *97*, 11279–11287. https://doi.org/10.1021/acs.analchem.5c01413.
18. Yuan, F.; Zhang, S.; Wang, Y.; et al. Activatable Near-Infrared Fluorescence Probe for Hypochlorous Acid Detection in Early Diagnosis of Keloids. *Anal. Chem.* **2024**, *96*, 16964–16970. https://doi.org/10.1021/acs.analchem.4c04201.
19. Zheng, H.; Peng, W.; Liu, M.; et al. Ratiometric Fluorescent Probe for Super-Resolution Imaging of Lysosome HClO in Ferroptosis Cells. *Anal. Chem.* **2024**, *96*, 11581–11587. https://doi.org/10.1021/acs.analchem.4c02435.
20. Zhang, X.; Yan, Y.; Peng, Q.; et al. A pH-sensitive multifunctional fluorescent probe based on *N*-annulated perylene for the sensitive and selective detection of hypochlorous acid. *Mater. Chem. Front.* **2017**, *1*, 2292–2298.
21. Zhang, Z.; Ma, L.; Huang, Y.; et al. A facile ratiometric near-infrared fluorescent probe using conjugated 1,8-naphthalimide and dicyanoisophorone with a vinylene linker for detection and bioimaging of hypochlorite. *Anal. Methods* **2023**, *15*, 3420–3425. https://doi.org/10.1039/d3ay00820g.
22. Maiti, A.; Manna, S.K.; Halder, S.; et al. Near-Infrared Fluorescent Turn-On Probe for Selective Detection of Hypochlorite in Aqueous Medium and Live Cell Imaging. *Chem. Res. Toxicol.* **2024**, *37*, 1682–1690. https://doi.org/10.1021/acs.chemrestox.4c00222.
23. Liang, Y.; Xu, T.; Xu, S.; et al. A HClO-activated BODIPY based ratiometric fluorescent probe with dual near-infrared channels for differentiating cancerous cells from normal cells and surgical guidance of tumor resection. *Biosens. Bioelectron.* **2025**, *275*, 117247. https://doi.org/10.1016/j.bios.2025.117247.
24. Lin, X.; Zhang, M.; Feng, H.; et al. Ratiometric Covalent Fluorescent Probes for Dynamic Super-Resolution Imaging of Mitochondrial HClO. *ACS Sens.* **2025**, *10*, 3713–3724. https://doi.org/10.1021/acssensors.5c00640.
25. Rehemaitijiang, M.; Li, G.; Zhu, R.; et al. Triple-Standard Hypochlorite Quantitative Array Enabled by Precise Stokes Shift Modulation in D-pi-A Chemodosimeters. *Anal. Chem.* **2025**, *97*, 9462–9470. https://doi.org/10.1021/acs.analchem.5c00821.
26. Cao, C.; Zhou, X.; Xue, M.; et al. Dual Near-Infrared-Emissive Luminescent Nanoprobes for Ratiometric Luminescent Monitoring of ClO^- in Living Organisms. *ACS Appl. Mater. Interfaces* **2019**, *11*, 15298–15305.
27. Jin, L.; Tan, X.; Dai, L.; et al. A highly specific and sensitive turn-on fluorescence probe for hypochlorite detection and its bioimaging applications. *RSC Adv.* **2019**, *9*, 15926–15932. https://doi.org/10.1039/c9ra01457h.
28. Liu, J.; Li, Z.; Peng, S.; et al. $ONOO^-$ Activatable Fluorescent Sulfur Dioxide Donor for a More Accurate Assessment of Cell Ferroptosis. *Anal. Chem.* **2024**, *96*, 2041–2051. https://doi.org/10.1021/acs.analchem.3c04565.
29. Karak, A.; Banik, D.; Ganguly, R.; et al. A Phenanthrenequinone-Based Ratiometric Fluorescent Probe for Rapid Detection of Peroxynitrite with Imaging in Osteoblast Precursor Cells. *Chem. Res. Toxicol.* **2024**, *37*, 771–778.
30. Wang, Z.; Yan, M.; Yu, M.; et al. A Fluorescent Probe with Zwitterionic ESIPT Feature for Ratiometric Monitoring of Peroxynitrite *In Vitro* and *In Vivo*. *Anal. Chem.* **2024**, *96*, 3600–3608. https://doi.org/10.1021/acs.analchem.3c05718.
31. Xie, H.; Zhang, J.; Chen, C.; et al. Sensitive and specific detection of peroxynitrite and in vivo imaging of inflammation by a “simple” AIE bioprobe. *Mater. Chem. Front.* **2021**, *5*, 1830–1835. https://doi.org/10.1039/D0QM01004A.
32. Gong, J.; Wang, X.; Wu, J.; et al. Diaminonaphthalene Boronic Acid (DANBA): New Approach for Peroxynitrite Sensing Site. *Angew. Chem. Int. Ed.* **2024**, *63*, e202409295. https://doi.org/10.1002/anie.202409295.
33. Chai, X.; Ma, X.; Sun, L.L.; et al. A Mitochondria-Targeting and Peroxynitrite-Activatable Ratiometric Fluorescent Probe for Precise Tracking of Oxidative Stress-Induced Mitophagy. *Anal. Chem.* **2024**, *96*, 20161–20168. https://doi.org/10.1021/acs.analchem.4c03759.
34. Kim, J.; Yoo, J.; Kim, B.; et al. An AIE-based fluorescent probe to detect peroxynitrite levels in human serum and its cellular imaging. *Chem. Commun.* **2024**, *60*, 5443–5446. https://doi.org/10.1039/d4cc01231c.
35. Gao, X.; Zhang, W.; Dong, Z.; et al. Multichannel, multifunctional ruthenium(II) complex luminescent probe for elucidating the relationship between peroxynitrite, ferroptosis, and Parkinson's disease. *Sens. Actuator B Chem.* **2025**, *428*, 137264. https://doi.org/10.1016/j.snb.2025.137264.
36. Wang, P.; Yu, L.; Gong, J.; et al. An Activity-Based Fluorescent Probe for Imaging Fluctuations of Peroxynitrite ($ONOO^-$) in the Alzheimer’s Disease Brain. *Angew. Chem. Int. Ed.* **2022**, *61*, e202206894. https://doi.org/10.1002/anie.202206894.
37. Huang, L.; Ma, L.; Zhu, Q.; et al. Visualizing Endoplasmic Reticulum Stress and Autophagy in Alzheimer's Model Cells by a Peroxynitrite-Responsive AIEgen Fluorescent Probe. *ACS Chem. Neurosci.* **2025**, *16*, 223–231.
38. Zhang, H.; Zhu, G.-N.; Xiang, F.-F.; et al. High-Throughput Screening of Antioxidant Drug Candidates from Natural Antioxidants with a “Zero” Intrinsic Fluorescence Peroxynitrite Sensing Precursor. *J. Med. Chem.* **2024**, *67*, 17855–17865. https://doi.org/10.1021/acs.jmedchem.4c01858.
39. Si, M.; Lv, L.; Shi, Y.; et al. Activatable Dual-Optical Molecular Probe for Bioimaging Superoxide Anion in Epilepsy. *Anal. Chem.* **2024**, *96*, 4632–4638. https://doi.org/10.1021/acs.analchem.3c05641.
40. Yang, W.; Liu, R.; Yin, X.; et al. Novel Near-Infrared Fluorescence Probe for Bioimaging and Evaluating Superoxide Anion Fluctuations in Ferroptosis-Mediated Epilepsy. *Anal. Chem.* **2023**, *95*, 12240–12246.
41. Chen, L.; Wu, X.; Yu, H.; et al. An Edaravone-Guided Design of a Rhodamine-Based Turn-on Fluorescent Probe for Detecting Hydroxyl Radicals in Living Systems. *Anal. Chem.* **2021**, *93*, 14343–14350.

42. Kang, Z.; Zhou, Y.; Wang, W.; et al. Dual-response chemosensor for monitoring changes of polarity and ·OH in ferroptosis of cell and zebrafish. Sens. *Actuator B Chem.* **2025**, *426*, 137121. https://doi.org/10.1016/j.snb.2024.137121.
43. Li, H.; Li, X.; Shi, W.; et al. Rationally Designed Fluorescence ·OH Probe with High Sensitivity and Selectivity for Monitoring the Generation of ·OH in Iron Autoxidation without Addition of H_2O_2. *Angew. Chem. Int. Ed. Engl.* **2018**, *57*, 12830–12834. https://doi.org/10.1002/anie.201808400.
44. Lee, J.; Kim, H.S.; Jangili, P.; et al. Fluorescent Probe for Monitoring Hydrogen Peroxide in COX-2-Positive Cancer Cells. *ACS Appl. Bio Mater.* **2021**, *4*, 2073–2079. https://doi.org/10.1021/acsabm.0c01135.
45. Long, Y.; Chen, J.; Zeng, F.; et al. An activatable NIR-II fluorescent probe for tracking heavy-metal ion and high-level salt-induced oxidative stress in plant sprouts. *Aggregate* **2023**, *4*, e288. https://doi.org/10.1002/agt2.288.
46. Hu, F.; Huang, Y.; Zhang, G.; et al. A highly selective fluorescence turn-on detection of hydrogen peroxide and d-glucose based on the aggregation/deaggregation of a modified tetraphenylethylene. *Tetrahedron Lett.* **2014**, *55*, 1471–1474. https://doi.org/10.1016/j.tetlet.2014.01.056.
47. Jiang, R.; Cai, Z.; Bai, H.; et al. Precise Modulation of the π-Conjugated Bridge of Naphthalimide-Based Probes for High-Performance Fluorescent Sensing of H_2O_2. *Anal. Chem.* **2025**, *97*, 11669–11677.
48. Zhao, W.; Zhang, S.; Yan, J.; et al. A dual-emission fluorescent probe for simultaneous detection of singlet oxygen and hypochlorous acid in lipid droplets. *Sens. Actuator B Chem.* **2024**, *412*, 135813. https://doi.org/10.1016/j.snb.2024.135813.
49. Wang, H.; Xiu, T.; Zhang, X.; et al. A Sequentially activated probe for simultaneous fluorescence imaging of ONOO⁻ and HOBr in brain to indicate Alzheimer's Disease. *Sens. Actuator B Chem.* **2025**, *440*, 137947. https://doi.org/10.1016/j.snb.2025.137947.
50. Murfin, L.C.; Weber, M.; Park, S.J.; et al. Azulene-Derived Fluorescent Probe for Bioimaging: Detection of Reactive Oxygen and Nitrogen Species by Two-Photon Microscopy. *J. Am. Chem. Soc.* **2019**, *141*, 19389–19396.
51. Mei, Y.; Hai, Z.; Li, Z.; et al. Dual-Responsive Near-Infrared BODIPY-Based Fluorescent Probe for the Detection of F^- and HClO in Organisms. *Anal. Chem.* **2024**, *96*, 3802–3809. https://doi.org/10.1021/acs.analchem.3c04856.
52. Fortibui, M.M.; Park, C.; Kim, N.Y.; et al. Dual-Emissive Detection of ATP and Hypochlorite Ions for Monitoring Inflammation-Driven Liver Injury *In Vitro* and *In Vivo*. *Anal. Chem.* **2024**, *96*, 9408–9415.
53. Kang, Z.; Zhou, Y.; Ma, Y.; et al. Dual-Site Chemosensor for Visualizing ·OH–GSH Redox and Tracking Ferroptosis-Inducing Pathways *In Vivo*. *Anal. Chem.* **2024**, *96*, 11932–11941. https://doi.org/10.1021/acs.analchem.4c01688.
54. He, L.; Wei, X.; Zhang, W.; et al. Fabrication of a Redox-Reversible Near-Infrared Fluorogenic Probe for Ferroptosis Process Monitoring and the Early Diagnosis of Diabetes. *Anal. Chem.* **2025**, *97*, 2411–2417.
55. Wu, W.-N.; Chen, X.; Liu, S.-S.; et al. A dual-response fluorescent hemicyanine probe for the detection of mitochondrial hypochlorite and viscosity based on ESIPT/AIE and TICT. *Sens. Actuator B Chem.* **2025**, *423*, 136695.
56. Li, B.; Peng, W.; Jin, Z.; et al. Development of a Near-Infrared Probe for Enhancing Cancer Therapy by Mitigating Pyroptosis-Induced Inflammation. *Anal. Chem.* **2025**, *97*, 5274–5282. https://doi.org/10.1021/acs.analchem.4c07048.
57. Zan, Q.; Fan, L.; Wang, R.; et al. Dual-channel fluorescent probe for simultaneously visualizing $ONOO^-$ and viscosity in epilepsy, non-alcoholic fatty liver and tumoral ferroptosis models. *Biosens. Bioelectron.* **2025**, *282*, 117495. https://doi.org/10.1016/j.bios.2025.117495.
58. Wei, D.; Dai, Y.; Yan, X.; et al. A Novel "Double-Responsive" and "Dual-Targeted" Multifunctional Fluorescent Probe Monitors the Level Changes of $ONOO^-$ in Mitochondria during Cell Pyroptosis. *ACS Sens.* **2025**, *10*, 2542–2553. https://doi.org/10.1021/acssensors.4c02841.
59. Wang, X.; Chen, Y.; Liu, C.; et al. An $ONOO^-$/Viscosity-Sensitive and Mitochondria-Targeted Near-Infrared Fluorophore for Real-Time Tracking Mitophagy and Photodynamic Therapy of *Cancer Anal. Chem.* **2025**, *97*, 10244–10251. https://doi.org/10.1021/acs.analchem.5c00104.